Therapeutic potential of red blood cell-derived extracellular vesicles in reducing neuroinflammation and protecting against retinal degeneration.

Rakshanya Sekar#[1], Adrian V. Cioanca#[1,2], Yilei (Evelyn) Yang[1] , Karthik Shantharam Kamath[3], Luke Carroll[3], Riccardo Natoli*[1,2], Yvette Wooff*[1,2].

[1] The John Curtin School of Medical Research, The Australian National University, Canberra, ACT, Australia.

[2] School of Medicine and Psychology, The Australian National University, Canberra, ACT, Australia

[3] Australian Proteome Analysis Facility, Macquarie University, NSW, Australia

#reflects equal first co-authorship

*reflects equal senior co-authorship

Corresponding author:

Email: yvette.wooff@anu.edu.au

Mobile: 0451845459

Keywords: Extracellular vesicles (EV); Red blood cell extracellular vesicles (RBC EV); Age-related macular degeneration (AMD); retinal degenerations; neurodegenerations; neuroinflammation; cell therapy; systemic administration.

Abstract:

Neuroinflammation is a pathological process mediated through immune cell activation and pro-inflammatory cytokine release, resulting in neuronal cell death. In the central nervous system (CNS), neuroinflammation is a characteristic feature underlying the onset and progression of retinal and neurodegenerative diseases. Targeting neuroinflammation to reduce neuronal cell death and protect against visual and cognitive declines is therefore a key therapeutic strategy. However, due to the complex and multi-faceted nature of these diseases, to date there has been little therapeutic success with single target approaches insufficient to tackle widespread and multi-pathway inflammatory cascades. Furthermore, as the retina and brain reside within immune-privileged environments, a major challenge in treating these diseases is producing and delivering a therapeutic that, in itself, does not exacerbate inflammation. Extracellular vesicles (EV), derived from red blood cells (RBC EV), present a promising solution to overcome these hurdles, due to their innate ability to cross blood-tissue barriers, biocompatible nature, and their broad anti-inflammatory properties to modulate complex neuroinflammatory pathways.

This study therefore investigated the therapeutic potential of RBC EV in mediating neuroinflammation using an *in-vivo* photo-oxidative damage model of retinal degeneration as a model for CNS neuroinflammation. In this work, we developed a novel incubation pipeline using N1 medium supplement and superoxide dismutase (SOD) supplementation to promote the production of safe, neuroprotective, and anti-inflammatory RBC EV. Delivery of RBC EV *in vivo*, was shown to be safe with strong penetration across all retinal layers. Further, therapeutic administration of RBC EV via local intravitreal injection significantly reduced inflammation and cell death and preserved retinal function. Notably, strong safety and therapeutic efficacy was also demonstrated in the retina following systemic (intraperitoneal) administration, highlighting a potential game-changing approach for less-invasive therapeutic delivery to the CNS. Finally, multi-omic analyses and *in vitro* findings supported an anti-inflammatory mechanism-of-action, with RBC EV modulating pro-inflammatory cytokine release, including those known to be involved in the pathogenesis of retinal and neurodegenerative diseases.

Taken together, these findings highlight the broad applicability of RBC EV in treating neuroinflammation in the CNS, presenting a scalable and effective treatment approach for these currently untreatable diseases.

Introduction:

Neuroinflammation within the central nervous system (CNS) plays a key role in the onset and progression of retinal and neurodegenerative diseases [1-3]. While the initial inflammatory response, including the activation of resident immune cells like microglia, aims to protect and repair neural tissue, prolonged immune cell activation and chronic inflammation ultimately results in neuronal cell death and the pathological decline of vision and cognitive functioning [4-6]. Therefore, developing therapeutics that can modulate neuroinflammatory pathways to prevent sustained inflammation and subsequent neuronal cell death holds strong potential for treating both retinal and neurodegenerative conditions [2, 7].

Challenges in developing therapeutics for both retinal and neurodegenerative diseases include overcoming blood-tissue barriers of these immune-privileged environments and modulating complex and multifaceted neuroinflammatory pathways [7-9]. The blood-brain barrier (BBB) and blood-retina barrier (BRB) exclude most therapeutics following systemic administration, necessitating invasive delivery methods [10]. These drugs are therefore often also encapsulated within synthetic nanoparticles, which can induce neurotoxicity [11] and provoke additional pro-inflammatory responses [12, 13]. Moreover, many drugs in development and clinical trials are designed to target single inflammatory pathways [14-16], which may be insufficient to address the multiple pathways involved in complex neurodegenerations such as Alzheimer's disease, Parkinson's disease and age-related macular degeneration (AMD) - a leading cause of blindness in the world [17]. As AMD alone affects 1:7 people over the age of 50, or 200M worldwide [18] with no widely available treatments [15, 16] , there is an urgent need to develop broadly anti-inflammatory and neuroprotective therapeutics to treat this, and other retinal and neurodegenerative diseases.

Extracellular vesicles (EV) offer a promising solution to overcome many of these challenges. Previously thought to be cellular debris, EV are now recognized as key players in both normal physiological processes and pathological conditions [19-22]. EV are ubiquitously distributed in bodily fluids and play essential roles in intercellular communication by transporting

bioactive molecules to adjacent and distant cell types to regulate biological pathways [23-25]. In fact, EV-mediated transport of molecular cargo has been shown in both the retina, and CNS to modulate inflammation across health and disease [20, 26-31]. Unlike synthetic nanoparticles, EV are cell-derived and offer higher biocompatibility [32], better biodistribution profiles [33], and low immunogenicity [34]; making them ideal therapeutic agents for treating neuroinflammation.

Red blood cell (RBC) derived EV are particularly ideal due to their inherent safety profile, homogeneity, and innate anti-inflammatory properties [35-37]. As mature RBCs do not have nuclear or mitochondrial DNA, RBC EV are less likely to carry bioactive molecules, reducing horizontal transfer [38]. With their abundant and homogenous nature, RBC are easy to collect and process in large quantities [39, 40], overcoming significant manufacturing hurdles associated with scale, homogeneity, and batch reproducibility as commonly seen with stem cell-based EV production [41]. Importantly, RBC EV express CD47 on their surface, inhibiting phagocytosis through interaction with the macrophage inhibitory receptor signal regulatory protein alpha (SIRPα), thus reducing RBC EV clearance and reducing adverse inflammatory reactions [42-45]. Notably, RBC EV have been shown to intrinsically induce anti-inflammatory effects in macrophages further enhancing their suitability for clinical applications in treating diseases of the brain and retina [40, 46]. The natural anti-inflammatory properties and clinical viability of RBC EV makes them ideal neuroinflammatory modulators for the CNS, which could be leveraged for the development of effective and biocompatible therapies for treating neurodegenerative disorders where neuroinflammation is an underlying feature, including AMD.

This study therefore aims to investigate the therapeutic potential of RBC EV in mediating neuroinflammation in the retina using an *in-vivo* photo-oxidative damage induced model of retinal degeneration [47]. The retina, as an extension of the CNS, displays similar anatomical, functional, and immunological aspects to the brain offering a valuable opportunity to study shared clinical and pathological features [48]. We have previously shown that mice undergoing photo-oxidative damage have increased levels of inflammation, initiating pathological changes such as immune cell activation and recruitment, and focal photoreceptor cell death [47] - hallmark features of currently incurable retinal degenerative diseases such as AMD.

134 In this study, we pioneered a unique incubation strategy to produce high yields of reproducible
135 anti-inflammatory and neuroprotective RBC EV, using N1 medium supplement and superoxide
136 dismutase (SOD). *In vivo* delivery of these RBC EV (N1+SOD), both locally and systemically,
137 was not only found to be safe, but showed strong therapeutic efficacy in protecting against
138 retinal degeneration, with RBC EV (N1+SOD) treated mice exhibiting reduced inflammation,
139 decreased retinal cell death, and preserved retinal function. Furthermore, using *in vitro* assays
140 and multi-omics analyses, we demonstrated that RBC EV (N1+SOD) were able to modulate
141 the release of key pro-inflammatory cytokines known to be involved in retinal degenerations,
142 such as IL-6 and IL-1β, supporting an anti-inflammatory mechanism-of-action likely
143 contributing to the observed retinal protection. These results combined supports the
144 development of RBC EV for the treatment of retinal degenerations and suggests broader
145 therapeutic applicability of RBC EV in modulating inflammation in the CNS, presenting a
146 scalable, effective, and potentially less-invasive systemic treatment approach for wider
147 neurodegenerative conditions.
148
149 **Methods:**
150
151 **2.1 Red blood cell (RBC) processing and characterisation**
152
153 ***2.1.1 RBC processing***
154
155 Whole mouse blood in EDTA was purchased from Applied Biological Products Management
156 (MSBX 0005 – 5ml tubes). Whole blood was spun at 600 xg for 20 minutes to separate the
157 plasma, buffy coat, and RBC. The plasma and buffy coat were removed via pipetting, and the
158 remaining RBC were diluted 1:10 in 1X PBS (Gibco; pH 7.2). RBC suspension was passed
159 through a leukocyte depletion filter (Sterile Acrodisc® WBC syringe filter with Leukosorb
160 Membrane, 25 mm; Pall) to remove contaminant leukocytes.
161
162 RBC suspension was incubated in T25 flasks supplemented with either: N1 Medium
163 Supplement (100X, Sigma; N6530) at 1:100 dilution and/or superoxide dismutase (SOD)
164 (Worthington Biochemicals; LS003540) at 5 ug/ml, Trans-resveratrol (Sigma PHR2201-
165 200MG), Kaempferol (Sigma, 60010-25MG) or L-Glutathione reduced (Sigma, G4251-1G)
166 for 18 hours at 37 °C on a shaker incubator at 90 rpm.
167

168 ***2.1.2 RBC health measurements:***

169

170 Post incubation, the RBC suspension was transferred to 15 mL falcon tubes and spun at 600xg
171 for 20 minutes to separate RBC from extracellular vesicles (EV) in suspension [36]. To
172 determine the effect of incubation on the health of RBC, the 600 xg pellet was resuspended in
173 1X PBS (Gibco; pH 7.2) in 1:1000-1:10000 dilution range to perform qualitative and
174 quantitative assessments. 200 µL of pellet suspension at 1:1000 was applied to a glass
175 hemocytometer (Westlab, product number 071301-9877) and the number of RBC in the large
176 centre square were counted to determine total cell number. Zeiss Axiovert 200 microscope was
177 used to take images of RBC at 4x and 20x magnification and images were processed using
178 ImageJ software (version 2.1.0). RBC abnormality percentage was determined by studying
179 RBC membrane and classifying them based on size (normal, microcyte and macrocyte) and
180 membrane shape variation (normal, burr cell, tear drop, sickle cell, ovalocyte and schistocyte),
181 all statistical analysis was performed on Prism 9.

182

183 ***2.1.3 RBC viability measurements:***

184

185 To determine the effect of supplementation on RBC viability post incubation, Calcein-AM
186 (C1430 , Thermo Fisher Scientific) and Annexin V (563973, BD Biosciences) staining was
187 performed and assessed using imaging flow cytometry (ImageStream®X MkII). Calcein-AM
188 was prepared as a stock solution of 10 mM in dimethyl sulfoxide (DMSO) and a working
189 solution of 100 µM in PBS buffer, pH 7.4 was prepared as required. 2×10^5 RBCs in 200 µl
190 PBS, were incubated for 45 minutes with Calcein-AM working solution (final concentration in
191 Calcein-AM, 5 µM) at 37°C in the dark to preserve fluorescence [49]. Cells were then spun
192 down by centrifugation (1000 xg at 4°C for 5 min), resuspended in 0.5 ml of Annexin V binding
193 buffer containing 2 mM calcium chloride and incubated with 5 µl Bv421-Annexin-V for 15
194 min at room temperature in the dark. Cells were analysed for biparametric histograms FL1
195 (Calcein-AM) versus FL2 (Annexin-V) using ImageStreamX Mk II (Amnis Corporation,
196 Seattle, WA, USA). RBC experimental permeabilization as a control of dying cells was readily
197 made with 1% saponin [50].

198

199 **2.2 RBC EV processing**

200

201 ***2.2.1 RBC EV isolation***

Following the 600 xg spin to remove RBC, the RBC supernatant was transferred to 15mL falcon tubes and spun at 1500 xg for 15 minutes and 3200 xg for 10 minutes, excluding the pellet at each spin step by transferring the supernatant to a fresh tube. Following, RBC supernatant S1 was transferred to ultracentrifuge tubes (Ultra-Clear Thinwall Tubes 13.2ml, Beckman Coulter, USA) and spun at 10,000 xg for 35 minutes. The resultant pellet P2 was discarded and the supernatant S2 was transferred to fresh ultracentrifuge tube and re-spun at 100,000 xg for 1h 30 minutes. P3 containing RBC EV was then collected, washed in PBS via tituration, and re-spun at 100,000 xg for 1h 35minutes. Finally, P4 (RBC EV pellet) was resuspended in 50-500uL (depending on downstream experiment) and/or snap-frozen at -80C until use.

2.2.2 RBC EV characterisation

NanoSight characterisation:

The concentration and size distribution of RBC EV was measured using nanoparticle tracking analysis on a NanoSight NS300 (Malvern Instruments, Malvern, United Kingdom) and/or ZetaView® QUATT (Particle Metrix, Ammersee, Germany) instrument. RBC EV were diluted 1:10,000 in 1x PBS to achieve a particle per frame value between 20 and 100. The mean concentration value for each sample, in particles/mL, was exported to Prism 9 for plotting and statistical analyses [20].

Cryogenic electron microscopy:

RBC EV samples (1:1000) in 1x PBS were applied to a glow-discharged (PELCO easiGlow™ Glow Discharge Cleaning System) 300 mesh EM grid with lacey carbon for vitrification at 80-90% humidity, in room temperature. Any excess sample present was removed by blotting with filter paper. Loaded grids were placed into liquid ethane (kept in equilibrium with solid ethane) using a Leica EMGP2 Automatic Plunge Freezer (Centre for Advanced Microscope facility, JCSMR) [51]. This grid was then stored in liquid nitrogen until further use. A JEOL JEM-F200 microscope was used to image EV at 200kV voltage and 16,000x magnification. Images were processed using ImageJ. All EV visible across 10 images were measured for size (in nanometres) and exported to Prism 9 for plotting and statistical analysis.

***Western blot analysis**:*

236 Total lysates were extracted from cells and RBC EV by incubating with RIPA buffer
237 supplemented with 1:100 protease inhibitor cocktail (Sigma-Aldrich, MO, United States). 10-
238 20 ug of protein lysates/well were separated on 4-12% polyacrylamide gels (Thermo Fisher
239 Scientific, MA, United States) at 100 V for 60 minutes and transferred to a Nitrocellulose
240 membrane (Bio-Rad, CA, United States) using a Power Blotter semi-dry system (Thermo
241 Fisher Scientific, MA, United States) at 20V for 15 minutes. Membranes were washed in PBS-
242 Tween (0.01%; PBS-T), blocked in Pierce™ Clear Milk Blocking Buffer (Thermo Fisher
243 Scientific, MA, United States) for 1 hour and then incubated overnight at 4°C with primary
244 antibodies TSG101 (1:1000, ab30871, Abcam, Cambridge, United Kingdom), ALIX (1:1000,
245 EPR23653-32, ab275377,Abcam, Cambridge, United Kingdom), Calnexin; CALX (1:1000,
246 ab22595, Abcam, Cambridge, United Kingdom) or GAPDH (1:2000, G9545-100UL, Sigma-
247 Aldrich, United States). Following three washes in PBS-T, blots were incubated in appropriate
248 secondary antibodies, HRP-conjugated Goat Anti-Rabbit IgG (H + L) (1:1000, 170-6515, Bio-
249 Rad, CA, United States) or Goat-anti-Mouse IgG (1:1000, 170-6516, Bio-Rad, CA, United
250 States) for 2 h at room temperature. Membranes were washed in PBS-T and developed for 2
251 min with ClarityTM Western ECL Substrate (Bio-Rad, CA, United States). Imaging was
252 performed using a ChemiDocTM MP Imaging System with Image LabTM software (Bio-Rad,
253 CA, United States).
254
255 ***2.2.3 RBC EV labelling***
256
257 To determine RBC EV uptake *in vivo* and *in vitro*, RBC EV were labelled using the SYTO™
258 RNASelect™ Green Fluorescent Cell Stain, a cell-permeant RNA-specific stain. The stain was
259 first diluted 1:5 in DMSO (#ICN19141880, Thermo Fisher Scientific, MA, United States) to
260 give a 1mM DMSO stock. The RBC EV stock was diluted in sterile 1x PBS to a total volume
261 of 100µL. 1x PBS was used as a control for background staining. 1µL of the DMSO stock was
262 then added to the diluted RBC EV, mixed thoroughly, and incubated at 37 °C for 30 minutes
263 (dark). At approximately halfway, the solutions were mixed to ensure the dye did not settle at
264 the bottom of the tube. Afterwards, the solutions were added to Amicon™ 50kDa MWCO filter
265 units (UFC505024, Merck) pre-rinsed with UltraPure™ distilled water, and spun at 5000xg for
266 20 minutes to remove excess unbound dye. The solutions were further washed thrice by adding
267 500µL of sterile 1x PBS and spinning the columns at 10,000xg for 10 minutes each time. The
268 solutions were then made up to the same volume using sterile 1x PBS. The fluorescently

labelled RBC EV or PBS-only control solutions were then used to determine RBC EV uptake *in vivo.*

2.2.4 RBC EV cell viability and inflammatory profiling

RBC EV (N1+SOD) in frozen -80 C aliquots were sent to CruxBioLabs (VIC, AUS) for independent validation of safety and anti-inflammatory properties using control and 100 ng/mL LPS (L6529-1MG, Thermo Fisher Scientific, MA,USA) stimulated human peripheral bone mononuclear phagocyte cells (50,000 PBMCs). Procartaplex (Thermo Fisher Scientific, MA, USA) custom panel 8-plex for IL-1α, IL-1β, IL-6, IL-8, IL-10, MCP-1, MIP-1α, TNFα according to the manufacturer's instructions (Cat# MCYTOMAG-70K, Merck Millipore, MA, USA).

2.3 Quantitative Proteomics on RBC and RBC EV

To characterize the proteomic signature of RBC and RBC EV with or without N1 and/or SOD supplementation, snap-frozen cell and EV pellets were used and processed by Australian Proteome Analysis Facility (APAF), Macquarie University, NSW, Australia. Protein concentrations were determined using a BCA assay. Fifty micrograms of protein from each sample were aliquoted and volumes were normalized with 100 mM TEAB and 1% SDC. Disulfide bonds were reduced with 10 mM DTT at 60 °C for 30 minutes and alkylated with 20 mM IAA at room temperature in the dark for 30 minutes. Proteins were digested with trypsin at a 1:25 enzyme-to-protein ratio for 16 hours at 37 °C. Subsequently, samples were acidified to 1% formic acid, centrifuged to pellet SDC, and the supernatant was desalted using Stage-Tip purification and dried via vacuum centrifugation. Reconstituted samples were diluted with 0.1% formic acid for LC-MS/MS analysis.

For ion-library creation using high pH RP-HPLC fractionation, a small portion of peptides from each sample were pooled, desalted using a C18 column, and dried. The peptide mixture was resuspended in 5 mM ammonia solution (pH 10.5), fractionated using an Agilent 1260 HPLC system over a 55-minute gradient, and consolidated into 20 fractions. Dried fractions were reconstituted in 0.1% formic acid for LC-MS/MS analysis.

LC-MS/MS analysis was performed using a Thermo Orbitrap Exploris mass spectrometer coupled with a Vanquish Neo UHPLC system. Peptides were trapped on a C18 PepMap 100 column and separated on a 75 µm × 30 cm C18 analytical column at 45 °C. The mobile phase consisted of 99.9% water with 0.1% formic acid (A) and 80% acetonitrile with 0.1% formic acid (B). Peptides were eluted over a linear gradient from 2.5% to 37.5% mobile phase B for 59 minutes at a flow rate of 300 nL/min. For Data-Dependent Acquisition (DDA) of HpH-fractionated samples, peptide precursors (350-1850 m/z) were scanned at 60k resolution with a 1.5 s cycle time and dynamic exclusion set to 15 seconds. Fragmentation was carried out using HCD at 27% normalized collision energy, and fragment ions were detected at 15k resolution. For Data-Independent Acquisition (DIA), peptides were eluted similarly, with MS1 scans at 60k resolution (350-1450 m/z) and MS2 scans at 30k resolution using 20 variable windows and 27% collision energy.

Data analysis was performed as previously described [27]. Raw DDA data were processed with FragPipe version 20.0 and MSFragger version 3.8 using a FASTA file containing *Mus musculus*, Bovine SOD, and decoy protein sequences (https://www.uniprot.org/, 55,022 sequences, 25-Aug-2023). Parameters included trypsin (semi-specific) with two missed cleavages, 20 ppm precursor and fragment mass tolerances, oxidation (M) as a dynamic modification, and carbamidomethyl (C) as a static modification. DIA data files were processed using DIA-NN version 1.8 with default parameters, using ion-library data generated from FragPipe. All DIA data files were loaded into DIA-NN, with output filtered at 0.01 FDR. Library precursors were reannotated using the FASTA database, enabling N-terminal methionine excision. Tryptic peptide digestion allowed a maximum of two missed cleavages. Peptide length was set between 7 and 30 residues, and precursor m/z ranged from 300 to 1800, with charge states between 1 and 4. Cysteine carbamidomethylation was a fixed modification, with a maximum of one variable modification.

2.3.2 Data analysis

Data analysis was performed as described previously [27]. The initial processing of protein intensity data began with the application of a base-2 logarithmic transformation excluding proteins with more than two missing values, within any single experimental group to maintain data integrity. For proteins with missing values, imputation strategy was employed. Post-imputation, data normalization was performed using variance stabilization transformation

(VST) via the normalize_vst function in the R DEP package, ensuring homoskedasticity. The processed data were then subjected to differential expression analysis following the limma pipeline, a well-established methodology in the field of bioinformatics for identifying differentially expressed genes or proteins with precision and reliability. Pathway analysis was conducted through gene set enrichment analysis (GSEA) utilizing the fgsea function using C2 canonical and C5 gene ontology database from the Molecular Signatures Database (MsigDB) serving as the reference gene sets.

Data tables for RBC and RBC-EV proteomics can be found in *Supplementary Table 1*

2.4 Gene Expression Analysis

2.4.1 RNA extraction

Small RNA extraction began with the lysis of RBC EV in 300 µL of lysis buffer, followed by the addition of 30 µL miRNA homogenate, and incubated on ice for 10 minutes. Subsequently, 330 µL Acid-Phenol:Chloroform was added, and the mixture was vortexed for 60 seconds. Centrifugation at 10,000xg for 5 minutes facilitated phase separation. The aqueous phase was transferred and mixed with 1.25x volume of ice-cold absolute ethanol for total RNA isolation. The mixture was then passed through a purification column. The column was washed with 700 µL miRNA wash solution #1 and twice with 500 µL wash solution #2, then spun dry. RNA was eluted with heated solution (95°C), collected into 30 µL, and stored at -80°C. RNA quality and concentration were measured using a Nanodrop ND-1000 spectrophotometer and Agilent 2100 Bioanalyzer.

2.4.2 Library preparation and sequencing

The library preparation for high-throughput sequencing of RNA from RBC EV was carried out at the Biomolecular Research Facility (JCSMR, ANU). Libraries were synthesized using the Capture and Amplification by Tailing and Switching (Diagenode). Libraries were sequenced on the Illumina NovaSeq 6000 acquiring at least 10 million 50bp single-end reads per sample as described previously [20].

2.4.3 Bioinformatics

Data analysis was performed as described in previous publication [20, 52]. For preprocessing-indexes, adapters, and template-switching oligonucleotides were removed with *cutadapt*. Subread-align was used of reads to the mm10 mouse genome following which *featureCounts* was run for quantifying miRNA alignments. The following command sequence voom --> lmFit --> ebayes --> topTable was used for assessing differential gene expression data in Rstudio using limma package.

The RNA data that support the findings of this study are openly available in the Sequencing Read Archive NCBI repository under bioproject reference number PRJNA1144155.

2.5 Animal Handling and Paradigms:

All experiments were conducted in accordance with the ARVO Statement for the Use of Animals in Ophthalmic and Vision Research and with approval from the Australian National University's (ANU) Animal Experimentation Ethics Committee (AEEC) (Ethics ID: A2020/41 and A2023/318; Rodent models and treatments for retinal degenerations). Adult male and female C57BL/6J wild-type (WT) mice (aged 60-80 postnatal days) were purchased from the Animal Resources Centre (ARC, Canning Vale, Western Australia (WA)). Mice were bred, reared, and housed under 12 h light/dark cycle conditions (5 lux) with free access to food and water.

Photo-oxidative damage (PD): Animals in the photo-oxidative damage group (PD) were placed into Perspex boxes coated with reflective interior surface and exposed to 100 K lux white light from light-emitting diodes (LED) for a period of 5 days and were administered a pupil dilator (Minims® atropine sulphate 1% w/v; Bausch and Lomb) to both eyes twice a day (9am and 4 pm) during the damage paradigm.

Dim-reared (DR) : Dim-reared control mice were maintained in standard housing conditions of 12 h light (5 lux)/dark cycle with free access to food and water.

Age-matched and sex-matched mice were randomly assigned to 5-day photo-oxidative damage (PD) or dim-reared control (DR) groups (N = 5-15 mice per group, each eye measured independently as biological replicate).

404

405 **2.6 *In vivo* administration of RBC EV**

406

407 To test safety and therapeutic efficacy of RBC EV, mice were administered with RBC EV both
408 locally and systemically in dim-reared (DR) or photo-oxidative damage (PD) conditions. Mice
409 were either injected with RBC EV (N1+SOD), RBC EV (SOD), RBC EV (N1), RBC EV
410 (PBS), or PBS (N1+SOD), PBS (SOD), PBS (N1) or PBS as controls. In some experiments,
411 RBC EV or PBS were labelled with SYTO RNASelect to fluorescently label EV RNA as per
412 above method. Mice from the same litter were used in each experiment for comparison and
413 were randomly assigned across treatment groups. Retinal function and morphological
414 assessments were performed using ERG, OCT and histology as listed in *2.5 Retinal*
415 *Assessment.*

416

417 ***2.6.1 Intravitreal injections***

418

419 Mice were anaesthetised with an intraperitoneal injection of Ketamine (100mg/kg) and Xylazil
420 (10mg/kg) and then 1% w/v Atropine was applied to the ocular surface of each eye to dilate
421 the pupils. Intravitreal injections were performed as described in detail previously [53]. A 10µL
422 NanoFil syringe, with a 34G needle was used to inject 1µL ($2.0x10^9$ EV) of each EV mixture
423 or control solution through the previously made pilot hole into the vitreous of the eye. After
424 injection, the eye was swabbed with 1% Chlorsig to prevent bacterial infection and GenTeal™
425 Gel to prevent eye dryness. To aid recovery, animals were intraperitoneally injected with
426 Reversamed (1mg/kg).

427

428 Animals were placed into photo-oxidative damage for 5 days (degeneration paradigm) or were
429 kept in standard housing conditions for 7 days (safety assessment).

430

431 ***2.6.2 Intraperitoneal injections:***

432

433 Mice were injected via intraperitoneal injection at $2.0x10^{11}$ EV/100µL dose daily for 5 days
434 (photo-oxidative damage) or were kept in standard housing conditions for 7 days (dim-reared
435 safety assessment).

436

437 **2.7 Retinal Assessment:**

438

439 ***2.7.1 Retinal function via electroretinography (ERG)***

440 Full-field scotopic electroretinography (ERG) was performed to assess the retinal function of
441 control or treated mice in DR conditions or following PD as described [54]. Mice were dark-
442 adapted overnight before being anaesthetised with an intraperitoneal injection of Ketamine
443 (100 mg/kg; Troy Laboratories, NSW, Australia) and Xylazil (6 mg/kg; Troy Laboratories,
444 NSW, Australia) diluted in PBS. Both pupils were dilated with one drop each of 2.5% w/v
445 phenylephrine hydrochloride and 1% w/v tropicamide (Bausch and Lomb, NY, USA).

446

447 Anaesthetised and pupil dilated mice (as above) were placed on the thermally regulated stage
448 of the Celeris ERG system (Diagnosys LLC, MA, USA) and response from both eyes was
449 simultaneously recorded as previously described [54]. Responses were recorded and analysed
450 using Espion V6 Software, (Diagnosys LLC, MA, USA). Statistics were performed in Prism
451 V9.4 (GraphPad Software, CA, USA) using a two-way analysis of variance (ANOVA) to test
452 for differences in a-wave and b-wave responses. Data were expressed as the mean wave
453 amplitude ± SEM.

454

455 ***2.7.2 Retinal tissue collection and preparation***

456 Animals were euthanised with CO2 following functional assessment. The superior surface of
457 the right eye from each animal was marked and enucleated, then immersed in 4%
458 paraformaldehyde (PFA) in PBS for 3 h at 4 °C. Eyes were then cryopreserved in 15% sucrose
459 solution overnight, embedded in OCT medium (Tissue Tek, Sakura, JP) and cryosectioned at
460 12 μm in a parasagittal plane (superior to inferior) using a CM 1850 Cryostat (Leica
461 Biosystems, Germany) [47, 54]. The retina from the left eye of each mouse was excised through
462 a corneal incision and placed into 300uL of Lysis/Binding Buffer (Thermo Fisher Scientific,
463 MA, USA) and stored at − 80 °C until further use.

464

465 ***2.7.3 TUNEL assay***

466

467 Terminal deoxynucleotidyl transferase (Tdt) dUTP nick end labelling (TUNEL) was used as a
468 measure of photoreceptor cell death. TUNEL in situ labelling was performed on cryosections
469 using a Tdt enzyme (Cat #3,333,566,001, Sigma-Aldrich, MO, USA) and biotinylated
470 deoxyuridine triphosphate (dUTP) (Cat #11,093,070,910, Sigma-Aldrich, MO, USA) as

471 previously described [47, 54]. Images of TUNEL stained sections were captured with the
472 A1 + confocal microscope at 20× magnification.
473
474 ***2.7.4 IBA-1 immunohistochemistry***
475
476 Immunolabeling for IBA-1 (1:1000, Anti-Iba1, Rabbit, 019-19741, Wako, Osaka, Japan) and
477 quantification was performed as previously described [47]. The number of IBA-1+ cells (a
478 marker of retinal microglia and macrophages) was counted across the superior and inferior
479 retina using two retinal sections per mouse and then averaged. Retinal cryosections were
480 stained with the DNA-specific dye bisbenzimide (1:10,000, Sigma-Aldrich, MO, United
481 States) to visualize the cellular layers. Images of IBA-1 + staining were captured with the
482 A1 + confocal microscope at 20× magnification.
483
484 **2.8 Imaging and statistical analysis**
485
486 Morphology of RBC was examined using Zeiss Axiovert 200 Fluorescence/Live cell imagine
487 microscope (Zeiss). Fluorescence in retinal sections was visualised using A1+ Confocal
488 Microscope System with NIS-Elements Advanced Research software.
489
490 RNA and Proteomic analysis: Statistical analysis for multiomics was performed as specified
491 above. Graphing was generated using ggplot2 package and Prism V9.0.
492
493 Functional analysis (ERG): All graphing and statistical analysis was performed using Prism 9
494 (GraphPad Software, CA, USA). Two-way analysis of variance (ANOVA) with Šídák or
495 Bonferroni multiple comparison post-hoc test was used to determine the statistical outcome; p
496 value of < 0.05 was considered statistically significant. All data were expressed as the
497 mean ± SEM.
498
499 Histology: All graphing and statistical analysis was performed using Prism 9 (GraphPad
500 Software, CA, USA). An unpaired Student t test, one-way analysis of variance (ANOVA), or
501 two-way ANOVA with Tukey's multiple comparison post-test were utilised to determine the
502 statistical outcome; p value of < 0.05 was considered statistically significant for all histological
503 analysis. All data were expressed as the mean ± SEM. For TUNEL and IBA counts, 2 sections

per mouse were used. If any section was partially missing due to cryosectioning, it was excluded from the analysis.

In vitro experiments: All graphing and statistical analysis was performed using Prism 9 (GraphPad Software, CA, USA). Unpaired t test, Mann–Whitney test with false discovery rate (FDR), or two-way ANOVA with Tukey's or Šídák multiple comparison post-hoc test was used to determine the statistical outcome. p value of < 0.05 was considered statistically significant.

In vivo experiments: 'N' represents the number of animals in the individual experimental run, graphs depict average of technical replicates from multiple measurements per animal.

516 **Results**

517

518 **Result 1: Media supplementation influences red blood cell (RBC) viability, profile, and**
519 **proteomic composition.**

520

521 To identify the optimal media supplementation for maintaining red blood cell (RBC) integrity,
522 RBC were isolated following plasma and leukocyte depletion and incubated overnight at 37°C
523 in 1:10 PBS, with or without the addition of culture supplements: N1 media supplement,
524 Superoxide Dismutase (SOD), N1+SOD, Resveratrol, Kaempferol, and Glutathione **(Figure**
525 **1A)**. Light microscopy was used to evaluate the membrane abnormalities of RBC post-
526 treatment to determine optimal supplementation dosage. Dilution curve analyses identified the
527 optimal supplementation dosage resulting in minimal membrane abnormalities: Resveratrol at
528 100 μM, Kaempferol at 2 μM, and Glutathione at 0.1 mM **(Supplementary Figure 1A,**
529 **P<0.05)**. These dosages were then re-evaluated against pre-treatment (Pre-Tx), PBS-only
530 control, N1 media supplement (1X), and/or SOD (5ug/mL). Resveratrol (100 μM), N1 media
531 supplement (1X) and/or SOD (5ug/mL) significantly reduced membrane abnormalities
532 compared to both pre-treatment and PBS-only control **(Figure 1B, P<0.05)**. Furthermore, RBC
533 counts were performed to quantify the preservation of cells post-incubation, with the RBC
534 (N1+SOD) group indicating the highest preservation and the RBC (Resveratrol, 100uM) group
535 the least **(Figure 1C, P<0.05),** compared to Pre-Tx. Hence, subsequent experiments progressed
536 with supplements N1 and/or SOD only.

537

538 To elucidate the effects of N1 and/or SOD on RBC viability, imaging flow cytometry was
539 performed to quantify the percentage of Calcein-positive (viability marker), Annexin-positive
540 (apoptosis marker), and double-positive cells. RBC treated with SOD alone displayed
541 comparable viability to that of Pre-Tx, followed by RBC treated with N1+SOD **(Figure 1D,**
542 **P<0.05)**. The gating strategy and representative images for imaging flow cytometry are
543 presented in **Supplementary Figure 1B-C**.

544

545 Following, the proteomic content of RBC (post-treatment) was analysed comparing between
546 supplement groups, PBS-only, and Pre-Tx control. PCA biplots, derived using the protein
547 expression values of all identified proteins, showed a large variation between treated groups,
548 in particular, compared to Pre-Tx samples **(Figure 1E, Supplementary Figure 2A-2B).** It was
549 also demonstrated that RBC with supplements each had uniquely expressed proteomic

550 composition, with RBC (N1) showing the highest number of uniquely expressed proteins
551 compared to RBC (PBS) samples **(Figure 1F)**. Finally, for pathway analysis of differentially
552 expressed proteins, PBS was first compared to Pre-Tx control, and this relative difference was
553 compared to each supplement group, identifying that proteins enriched in RBC (N1+SOD)
554 were involved in homeostasis, platelet activation, coagulation, and immune system regulation,
555 including innate immune system regulation **(Figure 1G).**
556
557
558
559
560
561
562
563
564
565
566
567
568
569
570
571
572
573
574
575
576
577
578
579
580

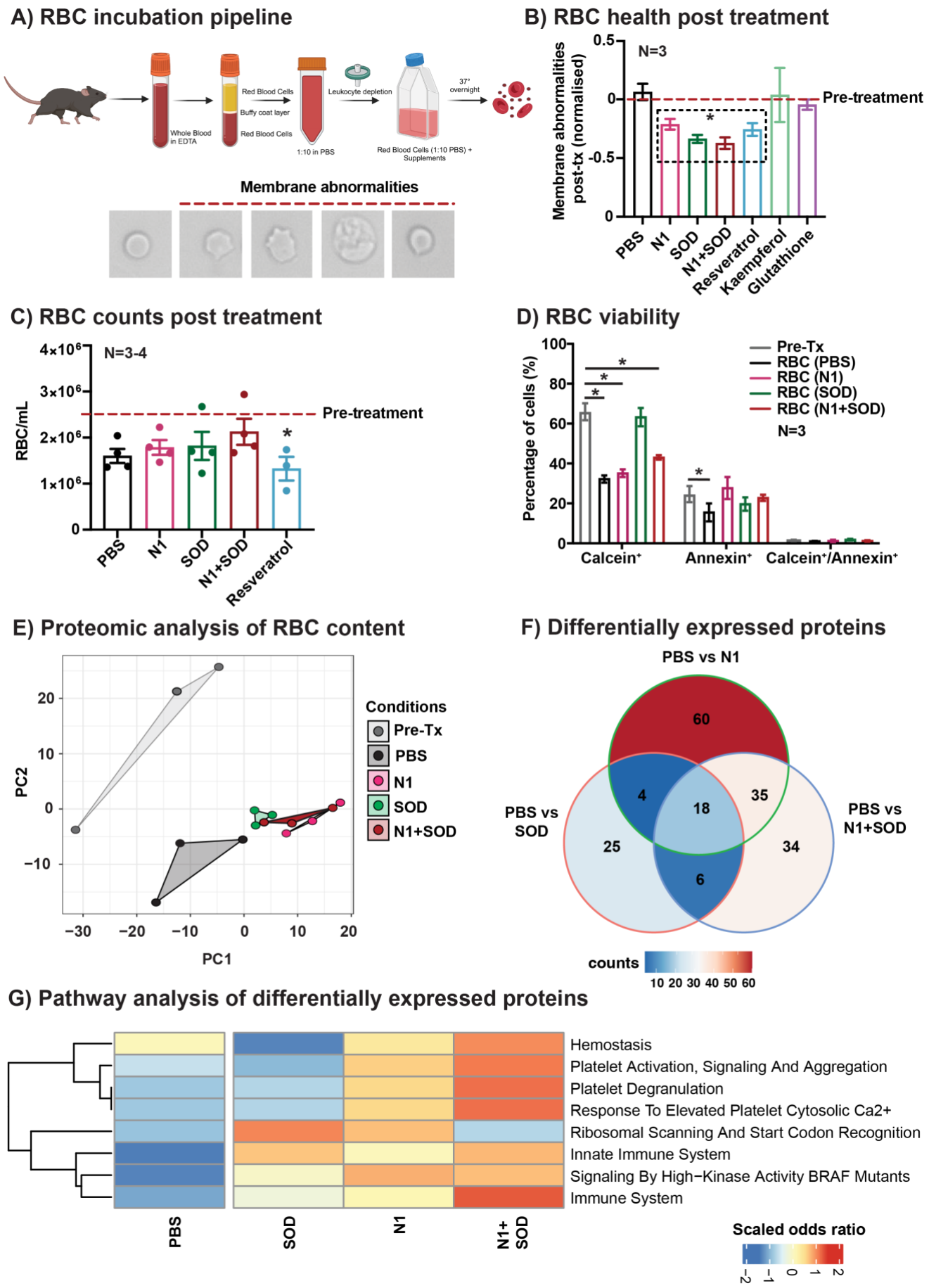
A) RBC incubation pipeline
Whole Blood in EDTA
Red Blood Cells
Buffy coat layer
Red Blood Cells
1:10 in PBS
Leukocyte depletion
Red Blood Cells (1:10 PBS) + Supplements
37° overnight
Membrane abnormalities
B) RBC health post treatment
Membrane abnormalities post-tx (normalised)
N=3
Pre-treatment
PBS
N1
SOD
N1+SOD
Resveratrol
Kaempferol
Glutathione
C) RBC counts post treatment
RBC/mL
N=3-4
Pre-treatment
PBS
N1
SOD
N1+SOD
Resveratrol
D) RBC viability
Percentage of cells (%)
Pre-Tx
RBC (PBS)
RBC (N1)
RBC (SOD)
RBC (N1+SOD)
N=3
Calcein+
Annexin+
Calcein+/Annexin+
E) Proteomic analysis of RBC content
PC2
PC1
Conditions
Pre-Tx
PBS
N1
SOD
N1+SOD
F) Differentially expressed proteins
PBS vs N1
PBS vs SOD
PBS vs N1+SOD
60
4
18
35
25
34
6
counts
10 20 30 40 50 60
G) Pathway analysis of differentially expressed proteins
Hemostasis
Platelet Activation, Signaling And Aggregation
Platelet Degranulation
Response To Elevated Platelet Cytosolic Ca2+
Ribosomal Scanning And Start Codon Recognition
Innate Immune System
Signaling By High−Kinase Activity BRAF Mutants
Immune System
PBS
SOD
N1
N1+ SOD
Scaled odds ratio

581
582

583 **Figure 1: Effects of media supplementation on RBC health, viability, and proteomic**
584 **content**. **(A)** Experimental paradigm: RBC population enriched from whole blood (EDTA)
585 following centrifugation and leukocyte depletion, then incubated in 1:10 PBS with
586 supplements**. (B)** RBC membrane abnormalities post-treatment compared to Pre-Tx control as
587 measured by light microscopy (N=3, $P<0.05$) **(C)** RBC counts post-treatment compared to Pre-
588 Tx control as measured by hemocytometer (N=3-4, $P<0.05$**) (D)** RBC viability post-treatment
589 compared to Pre-Tx control as measured using Amnis II imaging flow cytometry (N=3,
590 $P<0.05$). The proteomic content of RBC analysed using 1D LC-MS/MS, following which **(E)**
591 PCA showed a large variation between treated groups, in particular, compared to Pre-Tx
592 samples. **(F)** Venn diagram shows uniquely expressed proteins in supplement groups compared
593 to relative difference between PBS and Pre-Tx. **(G)** Heatmap displaying pathways associated
594 with proteins enriched in RBC groups compared to PBS controls (N=3).
595
596
597
598
599
600
601
602
603
604
605
606
607
608
609
610
611
612
613
614
615
616

617 **Result 2: Media Supplementation modulates proteomic signature and anti-inflammatory**
618 **properties of red blood cell-derived extracellular vesicles (RBC EV)**
619
620 Having demonstrated that supplementation can alter RBC health, viability, and proteomic
621 content, we investigated whether the N1 and/or SOD supplementation(s) have subsequent
622 effects on the RBC EV profile and molecular composition. Following overnight incubation, the
623 cell-free supernatant was processed using differential ultracentrifugation to obtain RBC EV
624 **(Figure 2A and Supplementary Figure 3A).** EV were then characterised using nanoparticle
625 tracking analysis which showed comparable size distribution profiles ranging between 100-400
626 nm **(Figure 2B)** irrespective of supplementation conditions. There was no significant change
627 in mean **(Figure 2Ci)** and mode **(Figure 2Cii)** size of RBC EV between the supplementation
628 conditions, however RBC EV (N1+SOD) generated significantly higher number of EV in
629 comparison to RBC EV (PBS), RBC EV (N1) and RBC EV (SOD) treatments **(Figure 2Ciii)**.
630 RBC EV (N1+SOD) were further characterised using cryogenic electron microscopy for size
631 and morphology **(Supplementary Figure 3B and 3C).** Western blotting was performed to
632 detect markers Calnexin (CNX), Tumor susceptibility gene 101 (TSG101) and ALIX (100
633 kDa). The CNX band (90 kDa) was observed in retinal lysates but was absent in RBC EV
634 lysates, indicating no cell contamination. **(Supplementary Figure 3D).** EV markers ALIX
635 were enriched in RBC EV fractions in comparison to RBC lysates **(Supplementary Figure**
636 **3E).** Multiple batches of RBC EV were tested for reproducibility by quantifying size and
637 profile using NTA **(Supplementary Figure 3F).**
638
639 Following characterisation, the proteomic composition of RBC EV was also explored. The
640 analysis revealed a comparable number of proteins across all groups – RBC EV (PBS), RBC
641 EV (N1), RBC EV (SOD), and RBC EV (N1+SOD) as shown in **Figure 2D**. However,
642 variations in protein composition were observed, with the RBC EV (N1+SOD) group
643 displaying the most variable expression profile compared to RBC EV (PBS), RBC EV (N1),
644 and RBC EV (SOD) groups (**Figure 2E)**. This was also reflected in the high number of unique
645 proteins found within this group **(Figure 2F)**. Pathway analysis of differentially expressed
646 (DE) proteins between these groups showed that, in the RBC EV (N1+SOD) group,
647 downregulated proteins were associated with several inflammatory pathways. These included
648 'interleukin 1 family signalling' and the 'non-canonical NfκB pathway,' as well as pathways
649 involved in the transcriptional regulation of inflammatory, apoptotic, mitotic, and
650 hematopoietic processes **(Figure 2G).**

Finally, small RNA sequencing was performed on RBC EV (PBS, N1, SOD and N1+SOD) groups to identify if there were any molecular changes in the microRNA signature as a response to supplementation. Out of the 260 total microRNA detected, it was identified that in all samples the top 11 microRNA were highly abundant and made up a significant fraction of the total reads, with RBC-enriched microRNA miR-451 found to be the most abundant **(Supplementary Figure 4A).** Pathway analysis of known targets of the top 11 microRNA identified regulation of processes such as transcription, biogenesis, and senescence **(Supplementary Figure 4B).** Venn diagram showed that there were no unique proteins between groups, suggesting that supplementation did not cause any changes to the microRNA signature of RBC EV **(Supplementary Figure 4C).**

Overall, these results support that media supplementation significantly affects the RBC EV profile and proteomic signature. Specifically, N1+SOD supplementation results in a higher EV concentration and distinct proteomic changes indicating an anti-inflammatory phenotype, more pronounced than other supplementation groups and controls, highlighting the unique impact of N1+SOD on RBC EV characteristics.

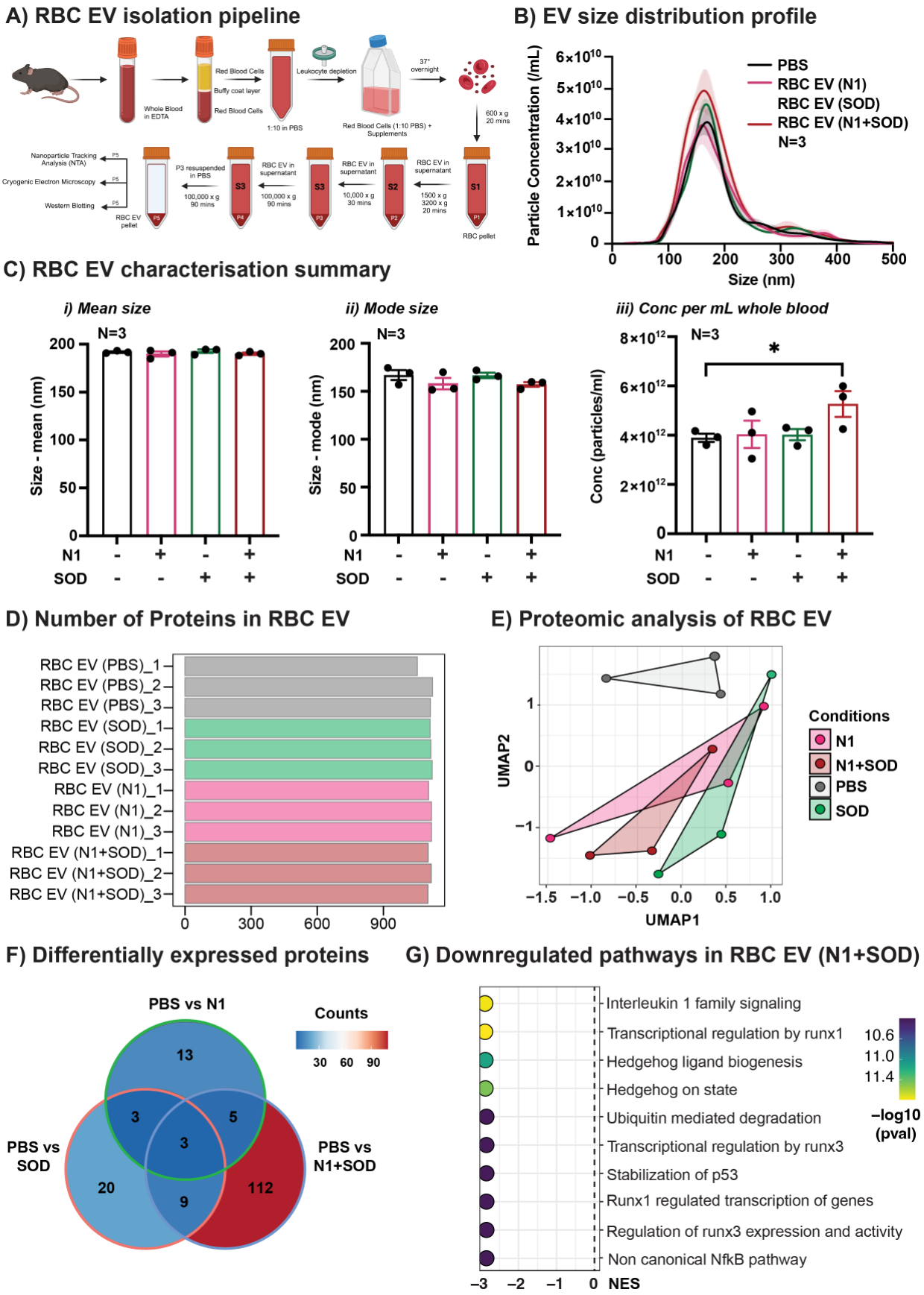
A) RBC EV isolation pipeline
Whole Blood in EDTA
Red Blood Cells
Buffy coat layer
Red Blood Cells
1:10 in PBS
Leukocyte depletion
Red Blood Cells (1:10 PBS) + Supplements
37° overnight
600 x g 20 mins
RBC pellet
RBC EV in supernatant
1500 x g 3200 x g 20 mins
10,000 x g 30 mins
100,000 x g 90 mins
P3 resuspended in PBS
RBC EV pellet
Nanoparticle Tracking Analysis (NTA)
Cryogenic Electron Microscopy
Western Blotting
B) EV size distribution profile
Particle Concentration (/mL)
Size (nm)
PBS
RBC EV (N1)
RBC EV (SOD)
RBC EV (N1+SOD)
N=3
C) RBC EV characterisation summary
i) Mean size
ii) Mode size
iii) Conc per mL whole blood
Size - mean (nm)
Size - mode (nm)
Conc (particles/ml)
N=3
N1
SOD
D) Number of Proteins in RBC EV
RBC EV (PBS)_1
RBC EV (PBS)_2
RBC EV (PBS)_3
RBC EV (SOD)_1
RBC EV (SOD)_2
RBC EV (SOD)_3
RBC EV (N1)_1
RBC EV (N1)_2
RBC EV (N1)_3
RBC EV (N1+SOD)_1
RBC EV (N1+SOD)_2
RBC EV (N1+SOD)_3
E) Proteomic analysis of RBC EV
UMAP1
UMAP2
Conditions
N1
N1+SOD
PBS
SOD
F) Differentially expressed proteins
PBS vs N1
PBS vs SOD
PBS vs N1+SOD
Counts
G) Downregulated pathways in RBC EV (N1+SOD)
Interleukin 1 family signaling
Transcriptional regulation by runx1
Hedgehog ligand biogenesis
Hedgehog on state
Ubiquitin mediated degradation
Transcriptional regulation by runx3
Stabilization of p53
Runx1 regulated transcription of genes
Regulation of runx3 expression and activity
Non canonical NfkB pathway
NES
−log10 (pval)

685
686

Figure 2: Effects of media supplementation on RBC EV profile and proteomic composition. **(A)** Experimental paradigm. RBC EV populations were isolated post-treatment using differential ultracentrifugation. **(B)** RBC EV size distribution profile post-treatment as measured using NTA (N=3)**. (C)** RBC EV (i) mean size, (ii) mode size and (iii) particle concentration/mL of whole blood as measured using NTA (N=3, $P<0.05$). Proteomic profile of RBC EV was examined using label-free 2D LC-MS/MS which showed **(D)** comparable numbers of proteins between treatment groups, but **(E)** distinct clustering between sample groups **(F)** Venn diagram represented uniquely expressed proteins within each group, highlighting the most numerous unique proteins were found in RBC EV (N1+SOD). **(G)** Pathway analysis identified that significantly downregulated proteins in RBC EV (N1+SOD) were associated with immune processes and transcriptional regulation (N=3, $P<0.05$).

720 **Result 3: Local delivery of RBC EV (N1+SOD) provides protection against retinal**
721 **degeneration.**
722
723 Given that the combination of N1 and SOD supplementation (N1+SOD) results in a higher
724 RBC EV concentration and distinct proteomic changes indicative of an anti-inflammatory
725 phenotype, we compared four supplementation strategies to identify the most effective *in-vivo*
726 candidate: RBC EV (N1), RBC EV (SOD), RBC EV (N1+SOD), and RBC EV (PBS). The
727 therapeutic efficacy of RBC EV derived from N1 and/or SOD supplementation was
728 investigated in a rodent model of retinal degeneration [47], using intravitreal administration
729 **(Supplementary Figure 5)**. Following 5 days of photo-oxidative damage, retinal function was
730 measured using ERG. Results demonstrated no significant change between the
731 supplementation groups for both a-wave **(Supplementary Figure 5A)** and b-wave
732 **(Supplementary Figure 5B)** responses. However, RBC EV (N1+SOD) showed significantly
733 reduced levels of photoreceptor cell death as measured by TUNEL assay **(Supplementary**
734 **Figure 5C, P<0.05)**, photoreceptor row counts **(Supplementary Figure 5D, P<0.05)**, and
735 retinal thickness measurements via OCT **(Supplementary Figure 5E-F, P<0.05)**, with
736 representative fundus images **(Supplementary Figure 5G, P<0.05)**.
737
738 Therefore, given the proteomics and above *in vivo* findings, the therapeutic efficacy of RBC
739 EV (N1+SOD) was further investigated against a PBS vehicle control **(Figure 3A)**, following
740 5 days of photo-oxidative damage. Results demonstrated that RBC EV (N1+SOD)-injected
741 mice had significantly preserved function for both a-wave **(Figure 3B, P<0.05)** and b-wave
742 **(Figure 3C; P<0.05)** responses compared to PBS-injected controls, along with significantly
743 reduced levels of photoreceptor cell death as measured by TUNEL assay **(Figure 3D, P<0.05)**
744 and photoreceptor row counts **(Figure 3E, P<0.05).** Further, RBC EV (N1+SOD)-injected
745 mice had significantly reduced numbers of IBA-1+ cells in the outer retina, indicating reduced
746 inflammatory cell presence **(Figure 3F; P<0.05)**. Representative confocal images illustrate
747 retinal protection against cell death and inflammation following local administration of RBC
748 EV (N1+SOD) (Figures 3G-H). TUNEL+ cells were also observed in the INL (Figure 3G),
749 with reduced overall INL signal in RBC EV (N1+SOD)-injected retinas compared to the PBS
750 vehicle control, however INL TUNEL+ cells were not quantified in this experiment.
751

Overall, these results support the protective and anti-inflammatory effects of RBC EV (N1+SOD), highlighting its potential as a therapeutic for retinal degeneration. This therapeutic not only reduces inflammation and cell death but also significantly preserves retinal function.

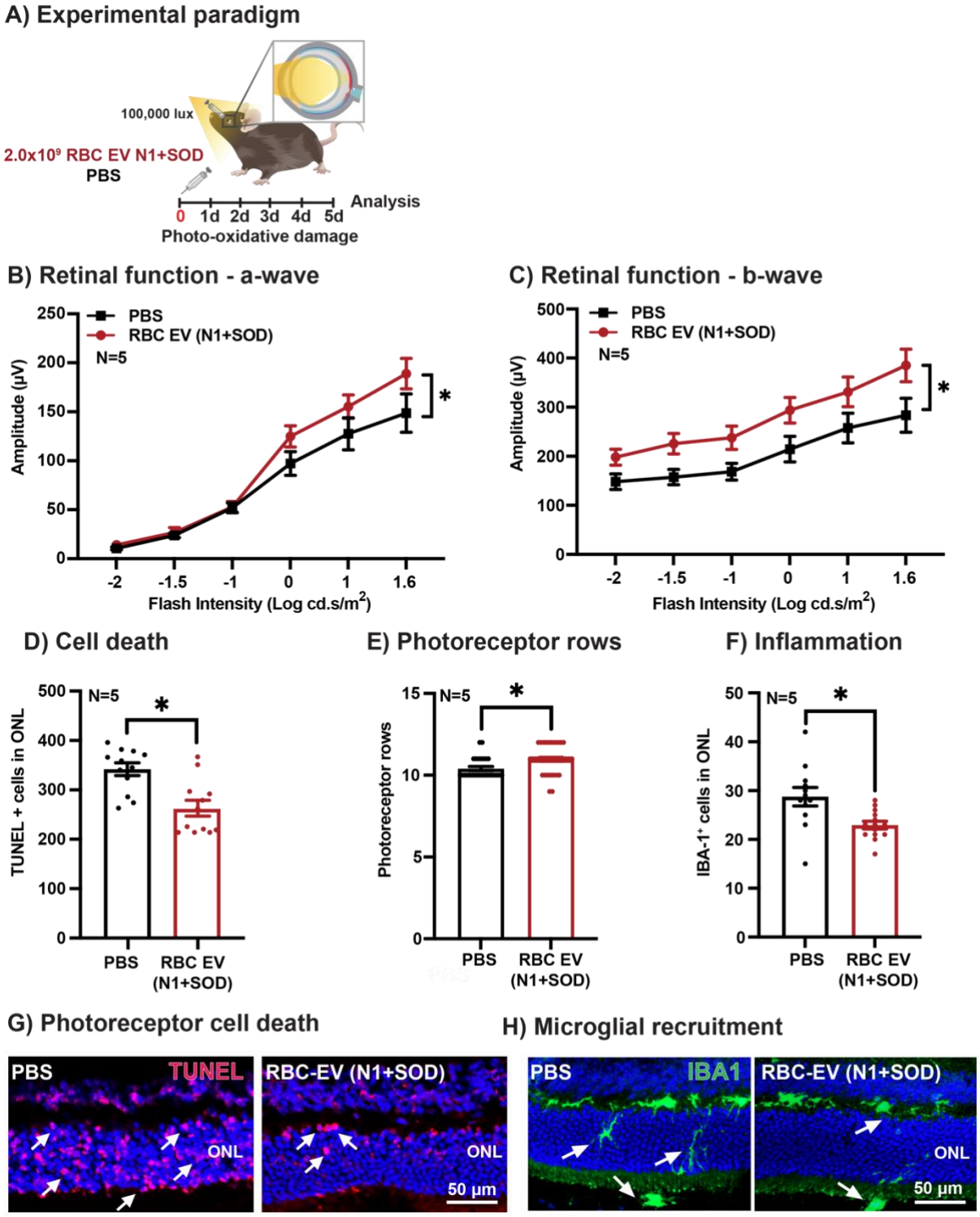
A) Experimental paradigm
100,000 lux
2.0x10⁹ RBC EV N1+SOD
PBS
0 1d 2d 3d 4d 5d
Analysis
Photo-oxidative damage
B) Retinal function - a-wave
PBS
RBC EV (N1+SOD)
N=5
Amplitude (µV)
Flash Intensity (Log cd.s/m²)
C) Retinal function - b-wave
PBS
RBC EV (N1+SOD)
N=5
Amplitude (µV)
Flash Intensity (Log cd.s/m²)
D) Cell death
N=5
TUNEL + cells in ONL
PBS
RBC EV (N1+SOD)
E) Photoreceptor rows
N=5
Photoreceptor rows
PBS
RBC EV (N1+SOD)
F) Inflammation
N=5
IBA-1⁺ cells in ONL
PBS
RBC EV (N1+SOD)
G) Photoreceptor cell death
PBS
TUNEL
ONL
RBC-EV (N1+SOD)
ONL
50 µm
H) Microglial recruitment
PBS
IBA1
RBC-EV (N1+SOD)
ONL
50 µm

792 **Figure 3: Therapeutic potential of local RBC EV delivery. (A)** Experimental paradigm for
793 intravitreal injections of RBC EV (N1+SOD). Retinal function as measured by ERG shows **(B)**
794 significantly preserved a-wave function and **(C)** b-wave function compared to PBS controls.
795 **(D)** $TUNEL^{+}$ cells in the ONL were significantly reduced in RBC EV (N1+SOD) compared to
796 controls, while **(E)** photoreceptor preservation was found to be significantly increased in RBC
797 EV (N1+SOD) compared to PBS. **(F)** IBA-1+ microglia were found to be significantly reduced
798 in RBC EV (N1+SOD) mice compared to PBS controls. **(G-H)** Representative confocal images
799 show decreased photoreceptor cell death and the presence of inflammatory cells in the outer
800 retina in RBC EV (N1+SOD) groups. (N=5, $P<0.05$). Scale = 50μM.
801

802 **Result 4: RBC EV (N1+SOD) is safely taken up across the retina following local delivery.**
803
804 Given the protective effects of N1+SOD supplementation, the safety of RBC EV (N1+SOD)
805 as a local therapeutic was assessed. Mice were injected with RBC EV (N1+SOD) using
806 intravitreal injection and left for 7 days in dim-reared condition **(Figure 4A)**. Retinal function
807 was measured using ERG, showing no significant difference in either a-wave **(Figure 4B)** and
808 b-wave responses **(Figure 4C)** compared to PBS injected controls (P>0.05). No differences
809 were observed for measures of cell death **(Figures 4D-E; P>0.05)**, or inflammation **(Figure**
810 **4F; P>0.05)**, as measured by TUNEL and IBA1, and shown in representative confocal images
811 **(Figures 4G)**. Minimal TUNEL signal was observed in the INL **(Figure 4G),** however INL
812 TUNEL+ cells were not quantified in this experiment. Overall, RBC EV (N1+SOD) did not
813 confer any toxicity or damage to the retina at the parameters measured, suggesting they can be
814 used as a safe therapeutic via local intravitreal injection.
815
816 In addition, to determine uptake efficiency of RBC EV (N1+SOD) in the retina, RBC EV
817 (N1+SOD) fluorescently labelled with SYTO RNASelect (green) were administered using
818 intravitreal injection. Retinal uptake *in vivo* was observed over 7 days following administration.
819 Uptake could be observed as early as 2 hours post-injection at the site of injection (superior
820 retina) and spread progressively radially across the retina (superior-inferior) as well as
821 penetrating through the retinal layers, with strong labelling observed within the ONL by 6 hours
822 and outer segment labelling from 48 hours. Labelling was still observed at 7 days throughout
823 the retina **(Figures 4H).**
824
825 These results support the use of RBC EV (N1+SOD) as a safe and effective therapeutic for
826 retinal degeneration, demonstrating strong uptake and distribution in the retina.
827
828
829
830
831
832
833
834
835

836

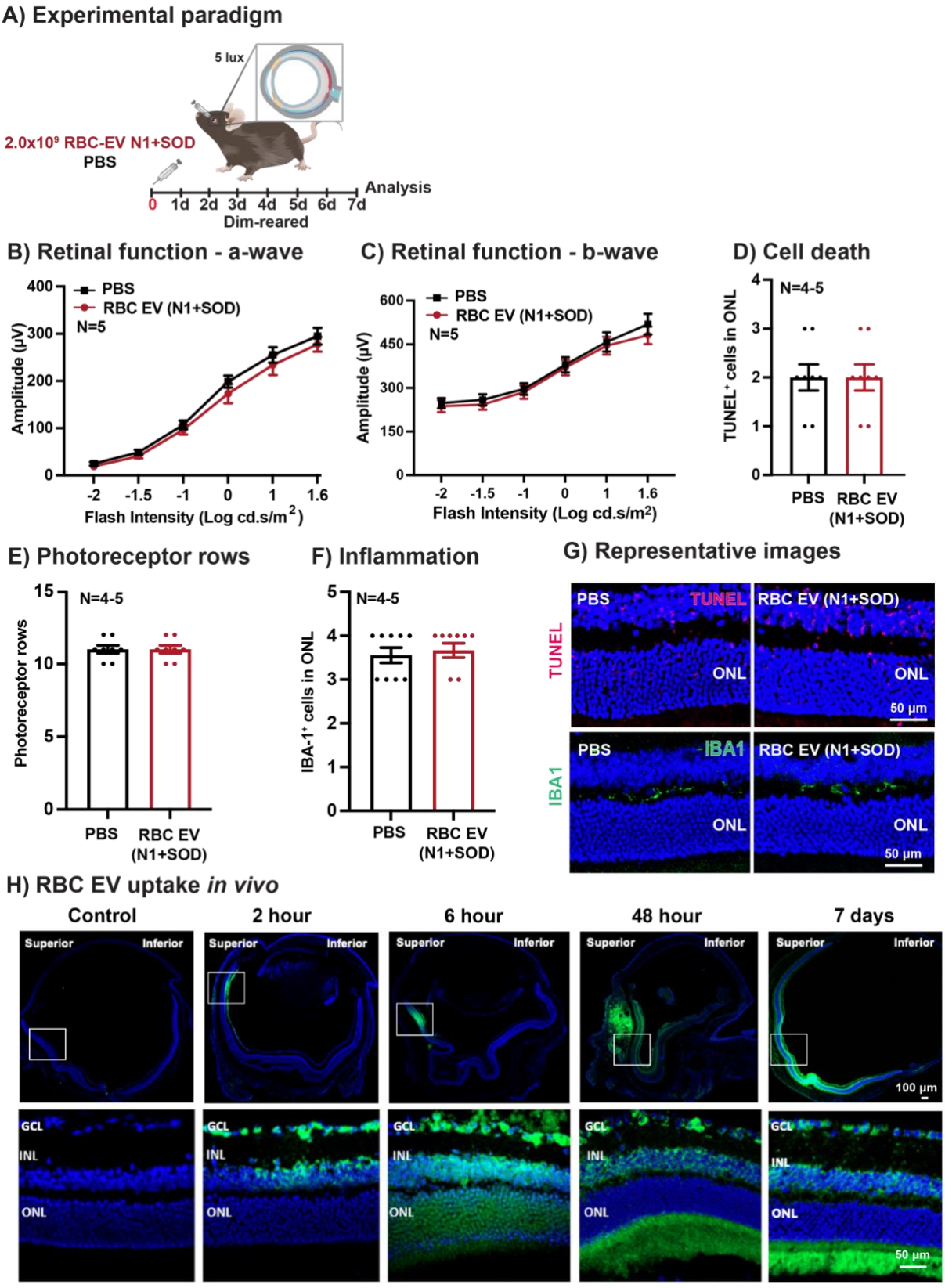

837
838
839
840
841

842 **Figure 4: Safety and distribution of local RBC EV (N1+SOD) delivery. (A)** Experimental
843 paradigm. Retinal function for both **(B)** a-wave and **(C)** b-wave responses was unchanged
844 compared to PBS-injected controls. Further, there were no significant differences in **(D)**
845 $TUNEL^+$ cells in the ONL, **(E)** number of photoreceptor rows, or **(F)** presence of $IBA\text{-}1^+$
846 microglia in the outer retina. **(G)** Representative confocal images show no differences in
847 $TUNEL^+$ cells and $IBA\text{-}1^+$ cells in outer retina between groups. (N=4-5, P>0.05). Scale =
848 50µM. **(H)** SYTO-labelled RBC EV (N1+SOD) (green) uptake *in vivo* following intravitreal
849 delivery over 7 days shows progressive radial uptake from the superior retinal delivery site, as
850 well as penetrance through all retinal layers and across the superior and inferior retina by 7
851 days. (N=1) ONL = outer nuclear layer, INL = inner nuclear layer, GCL = ganglion cell layer.
852 Scale bars = 100µm and 50µm.
853
854
855
856
857
858
859
860
861
862
863
864
865
866
867
868
869
870
871
872
873
874
875

Result 5-6 : Systemic delivery of RBC EV (N1+SOD) confers retinal protection against photo-oxidative damage and ensures retinal safety.

Following local delivery, to assess less-invasive delivery routes, systemic administration was explored for safety and therapeutic efficacy. The therapeutic efficacy of systemic RBC EV (N1+SOD) was investigated using daily intraperitoneal injections at a dose of 2.0×10^{11} EV/100µL over five days of photo-oxidative damage, compared to PBS control **(Figure 5A).** Retinal function measured using ERG showed significantly preserved retinal function in RBC EV (N1+SOD)-injected mice, for both a-wave **(Figure 5B; P<0.05)** and b-wave **(Figure 5C; P<0.05)** responses. Further, compared to PBS-injected controls, RBC EV (N1+SOD)-injected mice had significantly reduced levels of $TUNEL^{+}$ cells in the ONL **(Figure 5D; P>.0.5)**, significantly higher numbers of photoreceptor rows **(Figure 5E; P<0.05)**, and significantly reduced numbers of $IBA\text{-}1^{+}$ microglia/macrophages in the outer retina **(Figure 5F; P<0.05)**. Representative confocal images show decreased levels of cell death and inflammation in the retina of systemically injected RBC EV (N1+SOD) mice **(Figures 5G-H)**.

Similarly, the safety of systemic RBC EV (N1+SOD) administration was investigated by injecting the EVs daily for 7 days via intraperitoneal injection at a dose of 2.0×10^{11} EV/100µL, compared to PBS-injected controls **(Figure 6A).** Following 7 days of dosing under dim-reared condition, retinal function and morphological assessments were conducted. No significant differences were found in retinal function for a-wave **(Figure 6B; P>0.05)** or b-wave **(Figure 6C; P>0.05)** measures between groups. Additionally, there were no differences in levels of cell death **(Figures 6D-E; P>0.05)** or inflammation **(Figure 6F; P>0.05),** as shown in representative confocal images **(Figures 7G-H).**

In conclusion, systemic administration of RBC EV (N1+SOD) demonstrates a promising therapeutic potential for protecting the retina against degeneration. The treatment did not exhibit any signs of toxicity to the retina after 7 days of daily dosing, suggesting it is a safe and effective approach. These findings further support the investigation and development of RBC EV (N1+SOD) as a viable therapy for retinal protection.

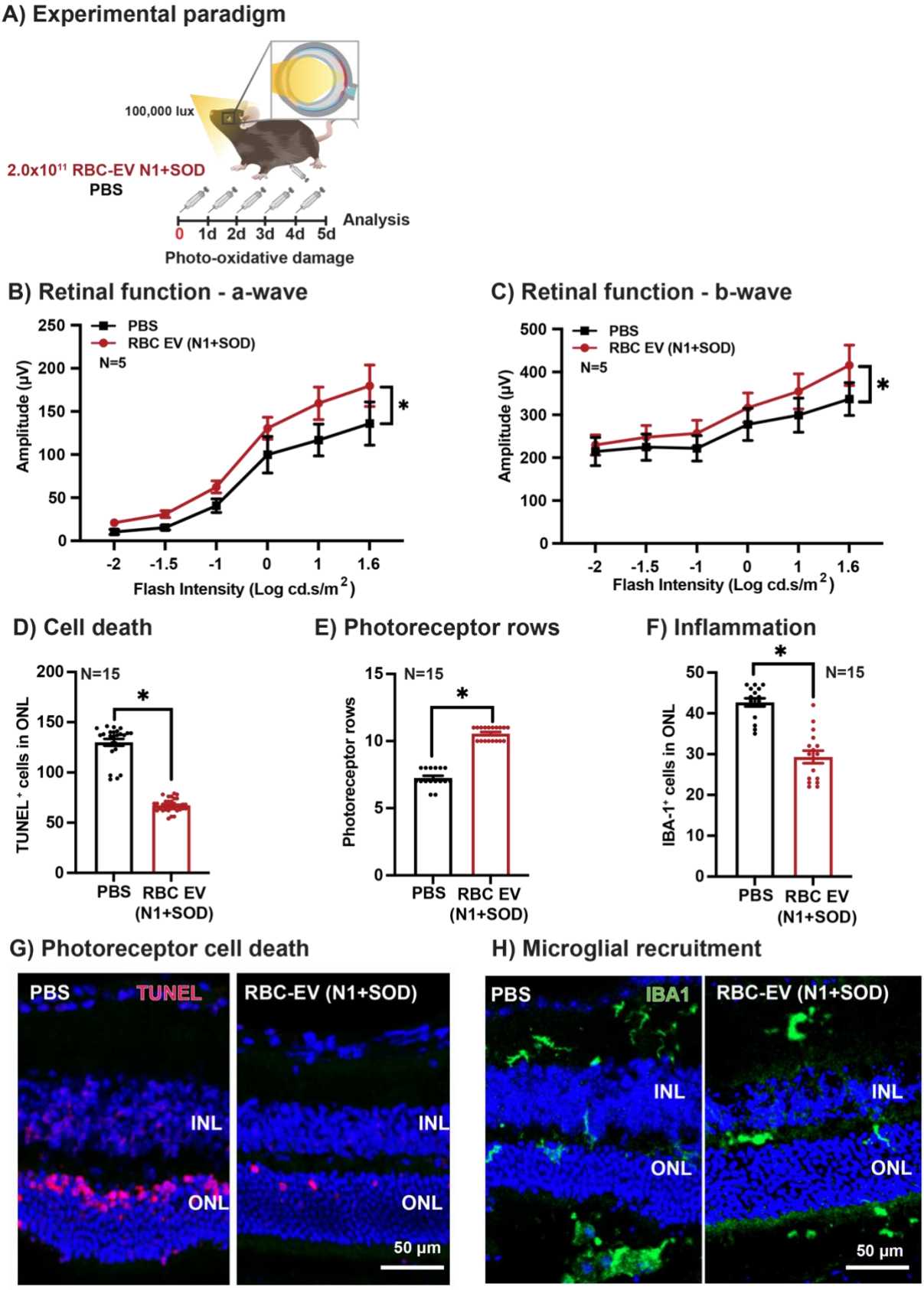
A) Experimental paradigm
100,000 lux
2.0x10¹¹ RBC-EV N1+SOD
PBS
0 1d 2d 3d 4d 5d
Analysis
Photo-oxidative damage
B) Retinal function - a-wave
PBS
RBC EV (N1+SOD)
N=5
Amplitude (µV)
Flash Intensity (Log cd.s/m²)
C) Retinal function - b-wave
PBS
RBC EV (N1+SOD)
N=5
Amplitude (µV)
Flash Intensity (Log cd.s/m²)
D) Cell death
N=15
TUNEL⁺ cells in ONL
PBS
RBC EV (N1+SOD)
E) Photoreceptor rows
N=15
Photoreceptor rows
PBS
RBC EV (N1+SOD)
F) Inflammation
N=15
IBA-1⁺ cells in ONL
PBS
RBC EV (N1+SOD)
G) Photoreceptor cell death
PBS
TUNEL
RBC-EV (N1+SOD)
INL
ONL
50 µm
H) Microglial recruitment
PBS
IBA1
RBC-EV (N1+SOD)
INL
ONL
50 µm

Figure 5: Therapeutic potential of systemic RBC EV (N1+SOD) delivery. (A) Experimental paradigm for intraperitoneal injections of RBC EV (N1+SOD). Retinal function as measured by ERG shows **(B)** significantly preserved a-wave function and **(C)** b-wave function compared to PBS controls (N=5, $P<0.05$). **(D)** $TUNEL^+$ cells in the ONL were significantly reduced in RBC EV (N1+SOD) compared to controls, while **(E)** photoreceptor preservation was found to be significantly increased in RBC EV (N1+SOD) compared to PBS. **(F)** IBA-1^+ microglia were found to be significantly reduced in RBC EV (N1+SOD) mice compared to PBS controls. **(G)** Representative confocal images show reduced $TUNEL^+$ cells in the ONL and preserved photoreceptor thickness in RBC EV (N1+SOD)-injected mice and **(H)** reduced IBA-1^+ cells in the outer retina, compared to PBS. (N=15, $P<0.05$). ONL = outer nuclear layer. Scale = 50μM.

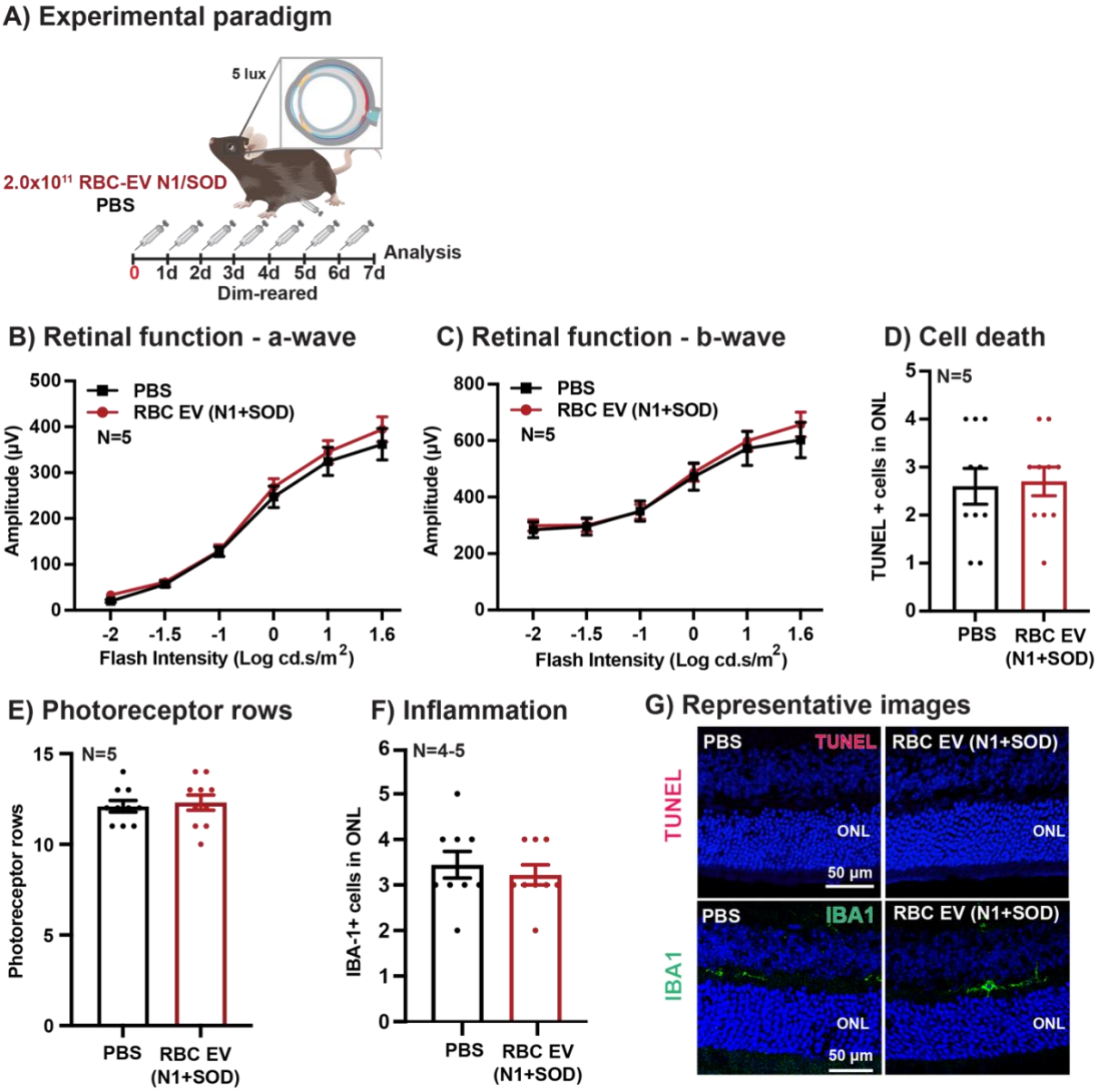
A) Experimental paradigm
5 lux
2.0x10¹¹ RBC-EV N1/SOD
PBS
Analysis
0 1d 2d 3d 4d 5d 6d 7d
Dim-reared
B) Retinal function - a-wave
PBS
RBC EV (N1+SOD)
N=5
Amplitude (µV)
Flash Intensity (Log cd.s/m²)
C) Retinal function - b-wave
PBS
RBC EV (N1+SOD)
N=5
Amplitude (µV)
Flash Intensity (Log cd.s/m²)
D) Cell death
N=5
TUNEL + cells in ONL
PBS
RBC EV (N1+SOD)
E) Photoreceptor rows
N=5
Photoreceptor rows
PBS
RBC EV (N1+SOD)
F) Inflammation
N=4-5
IBA-1+ cells in ONL
PBS
RBC EV (N1+SOD)
G) Representative images
TUNEL
IBA1
PBS
RBC EV (N1+SOD)
ONL
50 µm

Figure 6: Safety of systemic RBC EV (N1+SOD) delivery. (A) Experimental paradigm. Retinal function for both **(B)** a-wave and **(C)** b-wave responses was unchanged compared to PBS-injected controls. Further, there were no significant differences in **(D)** TUNEL$^+$ cells in the ONL, **(E)** the number of photoreceptor rows, or **(F)** presence of IBA-1$^+$ cells in the outer retina between groups. **(G-H)** Representative confocal images show no differences in TUNEL$^+$ cells and IBA-1$^+$ cells between groups. (N=4-5, P>0.05). ONL = outer nuclear layer. Scale = 50μM.

994 **Result 7: RBC EV (N1+SOD) have anti-inflammatory properties and can reduce**
995 **inflammatory cytokine release from PBMC.**
996
997 Finally, in order to assess and verify the observed immuno-modulatory properties of RBC EV
998 (N1+SOD) identified from multi-omic analyses and *in vivo* studies, RBC EV (N1+SOD) were
999 sent for independent validation for measures of metabolic activity, safety, and anti-
1000 inflammatory properties. RBC EV (N1+SOD) at 3 concentrations (1x, 0.3x and 0.01x, 1x=2.7
1001 x 10^{11}) were incubated on peripheral bone mononuclear phagocyte cells (50,000 PBMC/well)
1002 with inflammatory stimulation (LPS at 100 ng/mL). Further, dose responses were also
1003 evaluated. Cytokine outputs and viability measures were compared to control groups - PBS,
1004 PBS (N1+SOD), media, and dexamethasone 10nM.
1005
1006 Results suggested a dose-dependent increase in PBMC metabolic activity in response to
1007 increased RBC EV (N1+SOD) concentration in both control **(Supplementary Figure 6A)** and
1008 LPS-stimulated cells **(Supplementary Figure 6B)**.
1009
1010 RBC EV (N1+SOD) were also assessed for their safety profile on PBMCs, with cytokine output
1011 MIP-1α (CCL3), IL-1β, IL-6, IL-8 IL-10, TNFα, MCP-1 (CCL2) and IL-1α measured
1012 following 48 hours incubation **(Supplementary Figure 7).** These cytokines play known
1013 pathogenic roles in both retinal and neurodegenerative diseases [55-57]. While RBC EV
1014 (N1+SOD) increased basal inflammatory cytokine release over media control in the
1015 unstimulated condition, this was comparable to PBS and/or below the LLOQ (lower limit at
1016 which assay can provide quantitative results), with the exception of MCP-1 (CCL2) at 0.3x
1017 dose **(Supplementary Figure 7G)**. Overall, these results support broad safety of RBC EV
1018 (N1+SOD).
1019
1020 Following this, RBC EV (N1+SOD) were assessed for their anti-inflammatory properties using
1021 the same cytokine outputs and following 48 hours LPS stimulation and RBC EV (N1+SOD)
1022 incubation (**Figure 7A-H)**. Results showed an anti-inflammatory response for cytokines MIP-
1023 1α (CCL3), IL-1β and MCP-1 (CCL2), **(Figure 7A, B and G)**, with a dose-dependent decrease
1024 for cytokines MIP-1α (CCL3) and MCP-1 (CCL2). Importantly, RBC EV (N1+SOD) was able
1025 to reduce cytokine output below levels of anti-inflammatory steroid dexamethasone (10nM)
1026 for MIP-1α (CCL3) and MCP-1 (CCL2) **(Figure 7 A and G)**.

Taken together, these results collectively support the therapeutic use of RBC EV (N1+SOD) in reducing neuroinflammation and cell death, and in preserving retinal function through both local and systemic administration. The strong mechanism of action for RBC EV (N1+SOD) observed through omics, along with their ability to reduce release of key pro-inflammatory cytokines involved in retinal and neurodegenerative diseases, further highlights their potential as neuroinflammatory modulators.

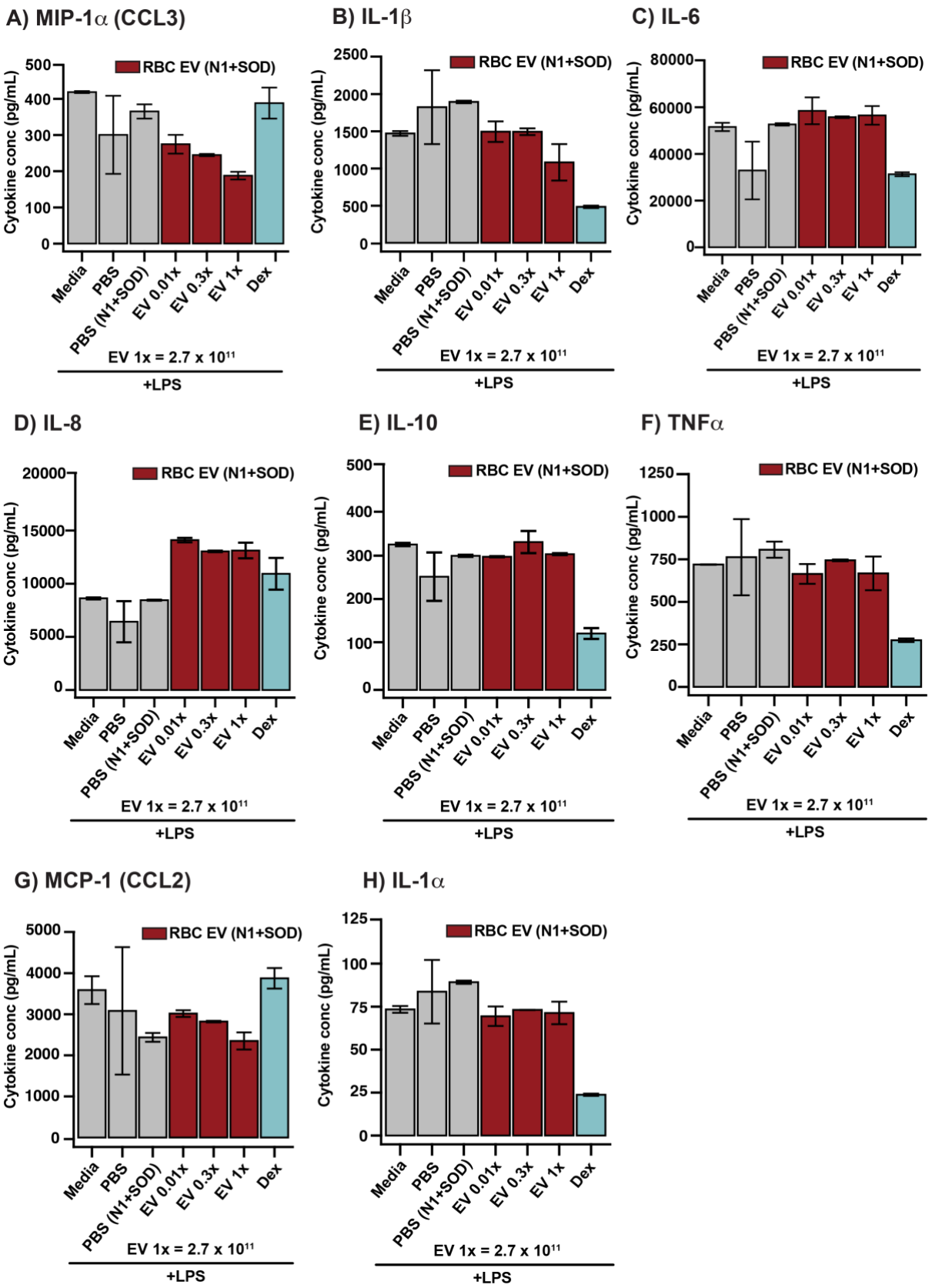
A) MIP-1α (CCL3)
B) IL-1β
C) IL-6
D) IL-8
E) IL-10
F) TNFα
G) MCP-1 (CCL2)
H) IL-1α
RBC EV (N1+SOD)
Cytokine conc (pg/mL)
Media
PBS
PBS (N1+SOD)
EV 0.01x
EV 0.3x
EV 1x
Dex
EV 1x = 2.7 x 10¹¹
+LPS

1059

1060

1061 **Figure 7: RBC EV (N1+SOD) decrease key pro-inflammatory cytokine production in**
1062 **PBMC. (A-H)** Cytokine output following incubation of LPS-stimulated PBMCs with RBC EV
1063 (N1+SOD) at 1x, 0.3x and 0.01x at 1x=2.7 x 10^{11}, for 48 hours, N=1, run in duplicates.
1064
1065
1066
1067
1068
1069
1070
1071
1072
1073
1074
1075
1076
1077
1078
1079
1080
1081
1082
1083
1084
1085
1086
1087
1088
1089
1090
1091
1092
1093
1094

Discussion

This study highlights the potential therapeutic application of RBC EV to mediate neuroinflammatory responses associated with retinal degenerations and suggests their broad applicability for treating retinal and neurodegenerative diseases where neuroinflammation is an underlying disease feature. We demonstrated that N1+SOD supplementation significantly influenced an anti-inflammatory RBC profile, resulting in a high-yield, reproducible, and neuroprotective RBC EV population. *In vivo*, local, and systemic administration of RBC EV (N1+SOD) provided significant protection against retinal degeneration, as demonstrated by significantly preserved retinal function, increased photoreceptor survivability, and decreased inflammation, while being safe with no signs of retinal toxicity. Additionally, *in vitro* cytokine assays strongly supported the anti-inflammatory mechanism-of-action observed *in vivo*, with RBC EV (N1+SOD) reducing the production of known pro-inflammatory cytokines involved in AMD and broader neurodegenerative diseases. Altogether, these findings demonstrate the use of RBC EV to modulate neuroinflammation and supports their broad applicability and exciting translational potential to be developed as less-invasive therapeutics for use in the CNS.

RBC EV (N1+SOD) are ideal therapeutics for treating neuroinflammation.

Neuroinflammation is a hallmark feature of retinal and neurodegenerative diseases, characterised by recruitment and activation of resident and peripheral immune cells, and pro-inflammatory cytokine release leading to neuronal cell death [2]. For the majority of retinal and neurodegenerative diseases, there are few, to no, treatments available. Given the significant contribution of inflammation to disease onset and progression, targeting inflammatory pathways to reduce the severity of disease is therefore a viable therapeutic strategy.

RBC EV have garnered significant interest as a lowly-immunogenic, and biologically compatible therapeutic with results from this work and others supporting their use in treating chronic inflammation [35-37, 40, 58]. Unlike stem cells and other primary cells in the body, as RBC do not have nuclear or mitochondrial DNA, RBC-EV have reduced molecular cargo limiting horizontal transfer and adverse effects in recipient cells and the development of oncogenic phenotypes [36, 43, 59, 60]. As the most abundant and non-inflammatory cell in the body, RBC can be readily collected and processed on a large scale for non-immunogenic EV, overcoming challenges of high costs and scalability associated with culturing and maintaining

primary cells for EV isolation [41, 61]. By utilising the body's own cells and natural communication pathways, these natural drug delivery vehicles can be readily collected from both patients and donors and redelivered as a safe autologous/allogenic therapeutic, improving patient safety and reducing adverse effects as a personalised treatment. In fact, RBC EV have previously demonstrated anti-inflammatory benefits in treating atherosclerosis, [40] and have shown therapeutic effects in various cancers, including metastatic breast cancer [36] and in models of cancer cachexia [37].

To improve upon the inherent protective qualities of RBC EV, in this work we showed that RBC EV (N1+SOD) derived using our novel incubation pipeline exhibited a unique anti-inflammatory and therapeutic profile compared to baseline RBC EV (PBS), or other supplementation conditions tested. The proteomic profile of RBC EV (N1+SOD) showed significant downregulation in proteins such as CRLF3, TOLLIP, EIF5, SNX15, WNK1 and GD1, which are involved in the transcription of pro-inflammatory genes, inflammasome-associated pathways, and interleukin-1 signalling [62-66]. This anti-inflammatory proteomic profile was further supported by anti-inflammatory microRNA cargo, including miR-451a and miR-let-7i-5p, which are known inhibitors of the TLR4/Nfκ-B inflammatory cascade [67]. This aligns with the significant therapeutic advantage of RBC EV (N1+SOD) *in vivo* over RBC EV (PBS) and other supplementation conditions in reducing neuroinflammation and neuronal cell death in the retina. We attribute this unique anti-inflammatory profile and improved protection against neuroinflammation to our incubation pipeline, which includes N1 medium components and superoxide dismutase (SOD). N1 medium components- transferrin, has previously been shown to reduce reactive oxidant species (ROS) formation [68], and progesterone, which conserves photoreceptors and reduces cell death in models of retinal degeneration along with SOD, which breaks down superoxide radicals; collectively enhancing neuroprotection [69]. We hypothesise that this combined approach mitigates excess ROS production, thereby protecting RBC during the incubation process to obtain high quality neuroprotective and anti-inflammatory EV, and to the retina during therapeutic delivery supporting RBC EV (N1+SOD) as an ideal therapeutic for treating neuroinflammation in retinal degenerations.

RBC EV (N1+SOD) reduced neuroinflammation in the retina

We showed in this work that RBC EV (N1+SOD) were able to modulate broad neuroinflammation by regulating the release of multiple pro-inflammatory cytokines,

addressing the need for multi-pathway modulation in these diseases. The marked reduction in pro-inflammatory cytokine levels - MIP-1α (CCL3), IL-1β, and MCP-1 (CCL2), is particularly significant as they play key roles in the onset and progression of various retinal and neurodegenerative conditions [12, 47, 54, 70-75]. MIP-1α (CCL3), expressed by astrocytes, glia, and neurons in the CNS, recruits circulating inflammatory cells to sites of damage, exacerbating inflammation and leading to neurodegeneration, including conditions like ischemic stroke, Alzheimer's disease, and various retinal degenerations such as neovascularization, ischemic retinopathy, and AMD [70, 71]. Similarly, IL-1β, a pleiotropic cytokine upregulated in Alzheimer's disease, Parkinson's disease, and AMD, activates microglia and astrocytes, stimulating the production of downstream pro-inflammatory cytokines [76]. Additionally, CCL2 controls the migration of monocytes/macrophages and dendritic cells [71, 74], and is involved in neurodegenerative disorders, including Alzheimer's disease, MS, and is significantly elevated in patients with both wet and dry AMD [47]. Our previous work has shown that reducing the expression of CCL3, CCL2, and IL-1β in the retina suppresses macrophage accumulation, decreases retinal inflammation and cell death [77, 78], supporting the protective mechanism of action of RBC EV (N1+SOD) observed *in vivo.* Furthermore, cytokines CCL2 and IL-1β are significantly upregulated in the early stages of retinal degeneration, preceding the onset of photoreceptor cell death [3], highlighting the potential of RBC EV (N1+SOD) as an early intervention for mitigating neuroinflammation and preserving tissue health before the onset of irreversible neuronal cell death in both retinal and neurodegenerative diseases.

Mechanism of systemic RBC EV (N1+SOD) administration for modulating neuroinflammation

Current challenges in developing therapeutics for combating neuroinflammation in the CNS include overcoming blood-tissue barriers including the BRB and BBB, which exclude most therapeutics following systemic administration. This challenge often necessitates more invasive delivery methods such as intravitreal delivery for retinal degenerations, or intracranial for neurodegenerations, both requiring specialised clinical care, and limiting the number of patients that can be treated due to a bottleneck in available specialists and higher costs [79]. RBC EV are a promising alternative, evidenced from the significant anti-inflammatory therapeutic effects seen when delivered systemically in this work.

We propose that systemic administration of RBC EV (N1+SOD) could provide therapeutic effects in the retina and wider CNS through several mechanisms. Firstly, EV have been shown to target and accumulate at sites of vascular damage [80], degeneration [81], or compromised blood-tissue barriers [82]. In the photo-oxidative damage model of retinal degeneration, which features compromised blood-tissue barriers and retinal cell death, this targeting ability suggests that anti-inflammatory RBC EV (N1+SOD) could provide localised protection to the retina following systemic administration. Secondly, RBC EV naturally target granulocytes, monocytes, and endothelial cells, which are crucial in maintaining the innate immune system within the CNS, which plays a key role in both retinal- and neurodegeneration [83]. RBC EV (N1+SOD) may target the innate immune system and circulating immune cells, preventing their infiltration into the retina and thereby mitigating degeneration. Additionally, RBC contain key complement-regulatory proteins, including CD55 and CD59, with previous studies showing AAV-mediated delivery of soluble CD59 (a C9 inhibitor) able to reduce membrane attack complex and NLRP3 inflammasome activation [84], both critical components of the innate immune system implicated in AMD [83]. Finally, as most EV types, including RBC EV, accumulate in the liver when delivered systemically, we hypothesise that local accumulation could provide anti-inflammatory effects due to the presence of phosphatidylserine (PS) on the EV plasma membrane [40]. PS, which is essential for neuron survival [85], has been previously shown to alter levels of pro-inflammatory cytokines in the brain when administered systemically, thereby boosting the central immune system against inflammatory insults [86]. In addition, as complement proteins are produced by the liver, we also hypothesise that systemic inhibition of liver-produced complement components may modulate circulating inflammation levels and induce a subsequent reduction in local retinal inflammation during degeneration [87, 88]. This hypothesis is supported from works showing the effects of liver produced complement proteins on inducing local complement activation in the eye [89]. The future development of this less-invasive approach would be a game-changer in the ophthalmic and neurodegenerative fields, reducing associated costs and increasing treatment accessibility to the wider population.

Conclusion

Neuroinflammation in the CNS significantly contributes to neurodegeneration, making it a critical target for therapeutic interventions aimed at treating retinal- and neurodegenerative diseases. Challenges in developing therapeutics for neuroinflammation include overcoming

blood-tissue barriers and modulating multiple neuroinflammatory pathways within immune-privileged environments. This study highlights the potential of RBC EVs (N1+SOD) in overcoming these challenges and effectively mediating neuroinflammation. We demonstrate that *in vivo* administration of RBC EVs (N1+SOD), both locally and systemically, preserved retinal function, increased photoreceptor survival, and reduced inflammation in a murine model of retinal degeneration. *In vitro* assays further support these neuro-modulatory effects by reducing pro-inflammatory cytokine production. These findings support the use of RBC EV (N1+SOD) for the treatment of retinal degenerations and broader neurodegenerative diseases, offering a scalable, effective, and less-invasive systemic treatment approach.

Author contributions

Rakshanya Sekar, Adrian V. Cioanca, Riccardo Natoli, and Yvette Wooff: conceptualization. Rakshanya Sekar, Adrian V. Cioanca, Yilei Yang, Karthik Kamath, Luke Carroll, and Yvette Wooff: methodology and data analysis. Rakshanya Sekar, Adrian V. Cioanca and Yvette Wooff: investigation. Rakshanya Sekar and Yvette Wooff: writing—draft, review, and editing. Riccardo Natoli and Yvette Wooff: funding acquisition. This research used NCRIS-enabled Australian Proteome Analysis Facility (APAF) infrastructure.

Conflict of interest statement

Rakshanya Sekar, Adrian V. Cioanca, Riccardo Natoli, and Yvette Wooff are inventors on an international PCT patent filed for this work (PCT/AU2024/050484). The remaining authors report no conflicts of interest.

Acknowledgements

An acknowledgement is made to the donors of the Macular Disease Research, a program of the BrightFocus Foundation (M2021012F), and to the Macular Disease Foundation Australia (MDFA), for support of this research awarded to Yvette Wooff, and to the ANU Impact Fund (IF601) and The National Health and Medical Research Council of Australia (NHMRC: 202239) awarded to Riccardo Natoli.

List of Abbreviations

AEC Animal Ethics Committee

1253 **AMD** Age related macular degeneration

1254 **cDNA** complementary DNA

1255 **CO2** Carbon dioxide

1256 **DR** Dim-reared

1257 **ERG** Electroretinography

1258 **EV** extracellular vesicle

1259 **HTS** high-throughput sequencing

1260 **INL** inner nuclear layer

1261 **LED** light-emitting diode

1262 **ONL** outer nuclear layer

1263 **PBS** phosphate buffered solution

1264 **PCA** principal component analysis

1265 **PD** Photo-oxidative damage

1266 **qPCR** quantitative polymerase chain reaction

1267 **RNA** ribonucleic acid

1268 **RT** room temperature

1269 **RBC EV** Red blood cell derived extracellular vesicles

1270 **SOD** Superoxide Dismutase

1271 **UMAP** Uniform Manifold Approximation and Projection

1272 **WT** Wild Type

1273

1274

References:

1. Zhang, W., et al., *Role of neuroinflammation in neurodegeneration development*. Signal Transduct Target Ther, 2023. **8**(1): p. 267.
2. Adamu, A., et al., *The role of neuroinflammation in neurodegenerative diseases: current understanding and future therapeutic targets*. Front Aging Neurosci, 2024. **16**: p. 1347987.
3. Wooff, Y., et al., *Short exposure to photo-oxidative damage triggers molecular signals indicative of early retinal degeneration*. Front Immunol, 2023. **14**: p. 1088654.
4. McGeer, P.L. and E.G. McGeer, *Inflammation and the degenerative diseases of aging*. Ann N Y Acad Sci, 2004. **1035**: p. 104-16.
5. Kwon, H.S. and S.H. Koh, *Neuroinflammation in neurodegenerative disorders: the roles of microglia and astrocytes*. Transl Neurodegener, 2020. **9**(1): p. 42.
6. Wyss-Coray, T. and L. Mucke, *Inflammation in neurodegenerative disease--a double-edged sword*. Neuron, 2002. **35**(3): p. 419-32.
7. Fornari Laurindo, L., et al., *Immunological dimensions of neuroinflammation and microglial activation: exploring innovative immunomodulatory approaches to mitigate neuroinflammatory progression*. Front Immunol, 2023. **14**: p. 1305933.
8. Jacquens, A., et al., *Neuro-Inflammation Modulation and Post-Traumatic Brain Injury Lesions: From Bench to Bed-Side*. Int J Mol Sci, 2022. **23**(19).
9. Muldoon, L.L., et al., *Immunologic privilege in the central nervous system and the blood-brain barrier*. J Cereb Blood Flow Metab, 2013. **33**(1): p. 13-21.
10. Wu, D., et al., *The blood-brain barrier: structure, regulation, and drug delivery*. Signal Transduct Target Ther, 2023. **8**(1): p. 217.
11. Nel, A., et al., *Toxic potential of materials at the nanolevel*. Science, 2006. **311**(5761): p. 622-7.
12. Potter, T.M., et al., *Analysis of Pro-inflammatory Cytokine and Type II Interferon Induction by Nanoparticles*. Methods Mol Biol, 2018. **1682**: p. 173-187.
13. Neun, B.W., A.N. Ilinskaya, and M.A. Dobrovolskaia, *Analysis of Complement Activation by Nanoparticles*. Methods Mol Biol, 2018. **1682**: p. 149-160.
14. den Heijer, J.M., et al., *A Phase 1B Trial in GBA1-Associated Parkinson's Disease of BIA-28-6156, a Glucocerebrosidase Activator*. Mov Disord, 2023. **38**(7): p. 1197-1208.
15. Heier, J.S., et al., *Pegcetacoplan for the treatment of geographic atrophy secondary to age-related macular degeneration (OAKS and DERBY): two multicentre, randomised, double-masked, sham-controlled, phase 3 trials*. Lancet, 2023. **402**(10411): p. 1434-1448.
16. Patel, S.B., et al., *Treatment of geographic atrophy: an update on data related to pegcetacoplan*. Curr Opin Ophthalmol, 2024. **35**(1): p. 64-72.
17. Flores, R., et al., *Age-Related Macular Degeneration: Pathophysiology, Management, and Future Perspectives*. Ophthalmologica, 2021. **244**(6): p. 495-511.
18. Mitchell, P., *Eyes on the future: a clear outlook on age-related macular degeneration*, in *Deloitte/Macular Degeneration Foundation Australia*. 2011.
19. Boulanger, C.M., G. Raposo, and C. Thery, *[Extracellular vesicles: How to pass in a few decades from a status of cellular debris, or worse, garbage bags, to that of inter-cellular messengers]*. Med Sci (Paris), 2021. **37**(12): p. 1089-1091.

20. Wooff, Y., et al., *Small-Medium Extracellular Vesicles and Their miRNA Cargo in Retinal Health and Degeneration: Mediators of Homeostasis, and Vehicles for Targeted Gene Therapy.* Front Cell Neurosci, 2020. **14**: p. 160.
21. Hill, A.F., *Extracellular Vesicles and Neurodegenerative Diseases.* J Neurosci, 2019. **39**(47): p. 9269-9273.
22. Yates, A.G., et al., *In sickness and in health: The functional role of extracellular vesicles in physiology and pathology in vivo: Part II: Pathology: Part II: Pathology.* J Extracell Vesicles, 2022. **11**(1): p. e12190.
23. Yim, K.H.W., et al., *Assessing Extracellular Vesicles in Human Biofluids Using Flow-Based Analyzers.* Adv Healthc Mater, 2023. **12**(32): p. e2301706.
24. Alberro, A., et al., *Extracellular Vesicles in Blood: Sources, Effects, and Applications.* Int J Mol Sci, 2021. **22**(15).
25. O'Grady, T., et al., *Sorting and packaging of RNA into extracellular vesicles shape intracellular transcript levels.* BMC Biol, 2022. **20**(1): p. 72.
26. Chan, B.D., et al., *Exosomes in Inflammation and Inflammatory Disease.* PROTEOMICS, 2019. **19**(8): p. 1800149.
27. Cioanca, A.V., et al., *Multiomic integration reveals neuronal-extracellular vesicle coordination of gliotic responses in degeneration.* J Extracell Vesicles, 2023. **12**(12): p. e12393.
28. Delpech, J.C., et al., *Neuroimmune Crosstalk through Extracellular Vesicles in Health and Disease.* Trends Neurosci, 2019. **42**(5): p. 361-372.
29. Gupta, A. and L. Pulliam, *Exosomes as mediators of neuroinflammation.* Journal of neuroinflammation, 2014. **11**: p. 68-68.
30. Marostica, G., et al., *Extracellular Vesicles in Neuroinflammation.* Frontiers in Cell and Developmental Biology, 2021. **8**.
31. Schnatz, A., et al., *Extracellular Vesicles in neural cell interaction and CNS homeostasis.* FASEB Bioadv, 2021. **3**(8): p. 577-592.
32. Murphy, D.E., et al., *Extracellular vesicle-based therapeutics: natural versus engineered targeting and trafficking.* Exp Mol Med, 2019. **51**(3): p. 1-12.
33. Ukidve, A., et al., *Erythrocyte-driven immunization via biomimicry of their natural antigen-presenting function.* Proc Natl Acad Sci U S A, 2020. **117**(30): p. 17727-17736.
34. Robbins, P.D. and A.E. Morelli, *Regulation of immune responses by extracellular vesicles.* Nat Rev Immunol, 2014. **14**(3): p. 195-208.
35. Pham, C.T., et al., *Red blood cell extracellular vesicles as robust carriers of RNA-based therapeutics.* Cell Stress, 2018. **2**(9): p. 239-241.
36. Usman, W.M., et al., *Efficient RNA drug delivery using red blood cell extracellular vesicles.* Nat Commun, 2018. **9**(1): p. 2359.
37. Peng, B., et al., *Red blood cell extracellular vesicles deliver therapeutic siRNAs to skeletal muscles for treatment of cancer cachexia*. Mol Ther, 2023. **31**(5): p. 1418-1436.
38. Anastasiadi, A.T., et al., *Exploring unconventional attributes of red blood cells and their potential applications in biomedicine.* Protein Cell, 2024. **15**(5): p. 315-330.
39. Klein, H.G., D.R. Spahn, and J.L. Carson, *Red blood cell transfusion in clinical practice.* Lancet, 2007. **370**(9585): p. 415-26.

40. Pham, T.T., et al., *Endocytosis of red blood cell extracellular vesicles by macrophages leads to cytoplasmic heme release and prevents foam cell formation in atherosclerosis*. J Extracell Vesicles, 2023. **12**(8): p. e12354.
41. Nieuwland, R., et al., *Reproducibility of extracellular vesicle research*. Eur J Cell Biol, 2022. **101**(3): p. 151226.
42. Belhadj, Z., et al., *A combined "eat me/don't eat me" strategy based on extracellular vesicles for anticancer nanomedicine*. J Extracell Vesicles, 2020. **9**(1): p. 1806444.
43. Chiangjong, W., et al., *Red Blood Cell Extracellular Vesicle-Based Drug Delivery: Challenges and Opportunities*. Front Med (Lausanne), 2021. **8**: p. 761362.
44. Khandelwal, S., N. Van Rooijen, and R.K. Saxena, *Reduced expression of CD47 during murine red blood cell (RBC) senescence and its role in RBC clearance from the circulation*. Transfusion, 2007. **47**(9): p. 1725-1732.
45. Hatherley, D., et al., *Paired receptor specificity explained by structures of signal regulatory proteins alone and complexed with CD47*. Mol Cell, 2008. **31**(2): p. 266-77.
46. Biagiotti, S., et al., *Extracellular Vesicles as New Players in Drug Delivery: A Focus on Red Blood Cells-Derived EVs*. Pharmaceutics, 2023. **15**(2).
47. Natoli, R., et al., *A model of progressive photo-oxidative degeneration and inflammation in the pigmented C57BL/6J mouse retina*. Exp Eye Res, 2016. **147**: p. 114-127.
48. Kaarniranta, K., et al., *Age-related macular degeneration (AMD): Alzheimer's disease in the eye?* J Alzheimers Dis, 2011. **24**(4): p. 615-31.
49. Bratosin, D., et al., *Novel fluorescence assay using calcein-AM for the determination of human erythrocyte viability and aging*. Cytometry A, 2005. **66**(1): p. 78-84.
50. Jacob, M.C., M. Favre, and J.C. Bensa, *Membrane cell permeabilization with saponin and multiparametric analysis by flow cytometry*. Cytometry, 1991. **12**(6): p. 550-8.
51. Yuana, Y., et al., *Cryo-electron microscopy of extracellular vesicles in fresh plasma*. J Extracell Vesicles, 2013. **2**.
52. Chu-Tan, J.A., et al., *Functional microRNA targetome undergoes degeneration-induced shift in the retina*. Mol Neurodegener, 2021. **16**(1): p. 60.
53. Gao, H., et al., *Safety of intravitreal voriconazole: electroretinographic and histopathologic studies*. Trans Am Ophthalmol Soc, 2003. **101**: p. 183-9; discussion 189.
54. Sekar, R., et al., *Impairing Gasdermin D-mediated pyroptosis is protective against retinal degeneration*. J Neuroinflammation, 2023. **20**(1): p. 239.
55. Kauppinen, A., et al., *Inflammation and its role in age-related macular degeneration*. Cellular and molecular life sciences : CMLS, 2016. **73**(9): p. 1765-1786.
56. Wooff, Y., et al., *IL-1 Family members mediate cell death, inflammation and angiogenesis in retinal degenerative diseases*. Frontiers in immunology, 2019. **10**: p. 1618.
57. Nagatsu, T. and M. Sawada, *Inflammatory process in Parkinson's disease: role for cytokines*. Curr Pharm Des, 2005. **11**(8): p. 999-1016.

58. Jayasinghe, M.K., et al., *Red Blood Cell-Derived Extracellular Vesicles Display Endogenous Antiviral Effects and Enhance the Efficacy of Antiviral Oligonucleotide Therapy.* ACS Nano, 2023. **17**(21): p. 21639-21661.
59. van der Vos, K.E., et al., *Brain tumor microvesicles: insights into intercellular communication in the nervous system.* Cell Mol Neurobiol, 2011. **31**(6): p. 949-59.
60. Chiangjong, W., et al., *Red Blood Cell Extracellular Vesicle-Based Drug Delivery: Challenges and Opportunities.* Frontiers in Medicine, 2021. **8**.
61. Estes, S., K. Konstantinov, and J.D. Young, *Manufactured extracellular vesicles as human therapeutics: challenges, advances, and opportunities.* Curr Opin Biotechnol, 2022. **77**: p. 102776.
62. Chen, K., et al., *Toll-interacting protein deficiency promotes neurodegeneration via impeding autophagy completion in high-fat diet-fed ApoE(-/-) mouse model.* Brain Behav Immun, 2017. **59**: p. 200-210.
63. Krueger, E.M., G.S. Miranpuri, and D.K. Resnick, *Emerging role of WNK1 in pathologic central nervous system signaling.* Ann Neurosci, 2011. **18**(2): p. 70-5.
64. Kowalski, E.J.A. and L. Li, *Toll-Interacting Protein in Resolving and Non-Resolving Inflammation.* Front Immunol, 2017. **8**: p. 511.
65. Huttenrauch, M., et al., *Glycoprotein NMB: a novel Alzheimer's disease associated marker expressed in a subset of activated microglia.* Acta Neuropathol Commun, 2018. **6**(1): p. 108.
66. Tan, T.C.J., et al., *Translation factor eIF5a is essential for IFNgamma production and cell cycle regulation in primary CD8(+) T lymphocytes.* Nat Commun, 2022. **13**(1): p. 7796.
67. Thomas, J.J., et al., *MiR-451a and let-7i-5p loaded extracellular vesicles attenuate heme-induced inflammation in hiPSC-derived endothelial cells.* Front Immunol, 2022. **13**: p. 1082414.
68. Duca, L., et al., *Non-transferrin-bound iron and oxidative stress during allogeneic hemopoietic stem cell transplantation in patients with or without iron overload.* Am J Hematol, 2018. **93**(9): p. E250-e252.
69. McCord, J.M. and I. Fridovich, *Superoxide dismutase. An enzymic function for erythrocuprein (hemocuprein).* J Biol Chem, 1969. **244**(22): p. 6049-55.
70. Marciniak, E., et al., *The Chemokine MIP-1alpha/CCL3 impairs mouse hippocampal synaptic transmission, plasticity and memory.* Sci Rep, 2015. **5**: p. 15862.
71. Yoshida, S., et al., *Role of MCP-1 and MIP-1alpha in retinal neovascularization during postischemic inflammation in a mouse model of retinal neovascularization.* J Leukoc Biol, 2003. **73**(1): p. 137-44.
72. Li, K., et al., *Anti-inflammatory and immunomodulatory effects of the extracellular vesicles derived from human umbilical cord mesenchymal stem cells on osteoarthritis via M2 macrophages.* J Nanobiotechnology, 2022. **20**(1): p. 38.
73. Rani, V., et al., *Role of pro-inflammatory cytokines in Alzheimer's disease and neuroprotective effects of pegylated self-assembled nanoscaffolds.* Curr Res Pharmacol Drug Discov, 2023. **4**: p. 100149.
74. Bose, S. and J. Cho, *Role of chemokine CCL2 and its receptor CCR2 in neurodegenerative diseases.* Arch Pharm Res, 2013. **36**(9): p. 1039-50.

75. Anand, A., et al., *Single nucleotide polymorphisms in MCP-1 and its receptor are associated with the risk of age related macular degeneration.* PLoS One, 2012. **7**(11): p. e49905.
76. Cahill, C.M. and J.T. Rogers, *Interleukin (IL) 1beta induction of IL-6 is mediated by a novel phosphatidylinositol 3-kinase-dependent AKT/IkappaB kinase alpha pathway targeting activator protein-1*. J Biol Chem, 2008. **283**(38): p. 25900-12.
77. Fernando, N., et al., *The broad-spectrum chemokine inhibitor NR58-3.14.3 modulates macrophage-mediated inflammation in the diseased retina*. J Neuroinflammation, 2016. **13**: p. 47.
78. Rutar, M., et al., *Chemokine-mediated inflammation in the degenerating retina is coordinated by Muller cells, activated microglia, and retinal pigment epithelium*. J Neuroinflammation, 2015. **12**: p. 8.
79. Ruiz-Moreno, J.M., et al., *Economic burden of age-related macular degeneration in routine clinical practice: the RAMDEBURS study.* Int Ophthalmol, 2021. **41**(10): p. 3427-3436.
80. Salybekov, A.A., et al., *Latest Advances in Endothelial Progenitor Cell-Derived Extracellular Vesicles Translation to the Clinic.* Front Cardiovasc Med, 2021. **8**: p. 734562.
81. Bang, O.Y. and J.E. Kim, *Stem cell-derived extracellular vesicle therapy for acute brain insults and neurodegenerative diseases*. BMB Rep, 2022. **55**(1): p. 20-29.
82. Kumar, M.A., et al., *Extracellular vesicles as tools and targets in therapy for diseases*. Signal Transduct Target Ther, 2024. **9**(1): p. 27.
83. Wong, J.H.C., et al., *Exploring the pathogenesis of age-related macular degeneration: A review of the interplay between retinal pigment epithelium dysfunction and the innate immune system*. Front Neurosci, 2022. **16**: p. 1009599.
84. Cashman, S.M., K. Ramo, and R. Kumar-Singh, *A non membrane-targeted human soluble CD59 attenuates choroidal neovascularization in a model of age related macular degeneration.* PLoS One, 2011. **6**(4): p. e19078.
85. Ma, X., et al., *Phosphatidylserine, inflammation, and central nervous system diseases*. Front Aging Neurosci, 2022. **14**: p. 975176.
86. Wang, C., et al., *Cerebral endothelial cell-derived extracellular vesicles regulate microglial polarization and promote autophagy via delivery of miR-672-5p.* Cell Death Dis, 2023. **14**(9): p. 643.
87. Kim, B.J., et al., *Targeting complement components C3 and C5 for the retina: Key concepts and lingering questions*. Prog Retin Eye Res, 2021. **83**: p. 100936.
88. Ong, J., et al., *The Complement System as a Therapeutic Target in Retinal Disease.* Medicina, 2024. **60**(6): p. 945.
89. Wu, J., et al., *Insights into the liver-eyes connections, from epidemiological, mechanical studies to clinical translation*. Journal of Translational Medicine, 2023. **21**(1): p. 712.